nature medicine

Article

https://doi.org/10.1038/s41591-024-02802-4

Therapeutic targeting of cellular senescence in diabetic macular edema: preclinical and phase 1 trial results

Received: 27 December 2022

Accepted: 3 January 2024

Published online: 06 February 2024

Check for updates

Sergio Crespo-Garcia[1,6], Frédérik Fournier[1], Roberto Diaz-Marin[1,2], Sharon Klier[3], Derek Ragusa[3], Lauren Masaki[3], Gael Cagnone[4], Guillaume Blot[1], Ikhlas Hafiane[2], Agnieszka Dejda[2], Rana Rizk[1], Rachel Juneau[2], Manuel Buscarlet[1], Sarah Chorfi[2], Priyanka Patel[3], Pedro J. Beltran[3], Jean-Sebastien Joyal[4], Flavio A. Rezende[2], Masayuki Hata[1], Alex Nguyen[3], Lynne Sullivan[3], Jason Damiano[3], Ariel M. Wilson[2], Frédérick A. Mallette[1,5], Nathaniel E. David[3], Anirvan Ghosh[3], Pamela R. Tsuruda[3], Jamie Dananberg[3] & Przemyslaw Sapieha[1,2,3] ✉

Compromised vascular endothelial barrier function is a salient feature of diabetic complications such as sight-threatening diabetic macular edema (DME). Current standards of care for DME manage aspects of the disease, but require frequent intravitreal administration and are poorly effective in large subsets of patients. Here we provide evidence that an elevated burden of senescent cells in the retina triggers cardinal features of DME pathology and conduct an initial test of senolytic therapy in patients with DME. In cell culture models, sustained hyperglycemia provoked cellular senescence in subsets of vascular endothelial cells displaying perturbed transendothelial junctions associated with poor barrier function and leading to micro-inflammation. Pharmacological elimination of senescent cells in a mouse model of DME reduces diabetes-induced retinal vascular leakage and preserves retinal function. We then conducted a phase 1 single ascending dose safety study of UBX1325 (foselutoclax), a senolytic small-molecule inhibitor of BCL-xL, in patients with advanced DME for whom anti-vascular endothelial growth factor therapy was no longer considered beneficial. The primary objective of assessment of safety and tolerability of UBX1325 was achieved. Collectively, our data suggest that therapeutic targeting of senescent cells in the diabetic retina with a BCL-xL inhibitor may provide a long-lasting, disease-modifying intervention for DME. This hypothesis will need to be verified in larger clinical trials. ClinicalTrials.gov identifier: NCT04537884.

Diabetic retinal disease, a persistent complication of diabetes, is characterized by degeneration of retinal neurovascular units[1,2] and remains one of the leading causes of blindness in working-age populations worldwide[3]. The retina is finely vascularized to support the elevated energetic demand required for vision[4]. Consequently, the neural retina and its blood vessels are particularly vulnerable to metabolic perturbations such as in diabetic retinopathy (DR). DR can be broadly characterized by an early stage of non-proliferative diabetic retinopathy (NPDR)

A full list of affiliations appears at the end of the paper. ✉e-mail: mike.sapieha@umontreal.ca

with clinical features that include microaneurysms, hemorrhages and intraretinal microvascular abnormalities. A more advanced stage of DR consists of proliferative diabetic retinopathy (PDR), associated with pathological preretinal neovascularization[5]. At various stages of DR, breakdown of the blood–retina barrier (BRB) leads to diabetic macular edema (DME) where extravasation of plasma and circulating proteins into the intraretinal and subretinal spaces causes swelling and subsequent vision loss.

Current standards of care for DME involve anti-vascular endothelial growth factor (VEGF) agents. These treatments effectively improve visual acuity and reduce macular edema, with the majority of the effect observed within the first 6 months of treatment[6]. However, the response is suboptimal in a large proportion of patients[7,8], and the efficacy can diminish over time[5]. In addition, with protracted use of intravitreal anti-VEGF agents, retinal liabilities have been reported in age-related macular degeneration (AMD)[9,10], which are in agreement with rodent studies that have predicted neuronal toxicity[11] and degeneration of retinal pigment epithelium–choriocapillaris complexes[12–14]. Corticosteroids, while effective at reducing edema, can trigger a rise in intraocular pressure (IOP) as well as cataracts[15]. Grid/focal laser therapy scars and seals leaky vessels but can also irreparably damage the retina[16]. Finding alternative safe, long-lasting and disease-modifying therapies for DME will benefit patients.

While DR is of multifactorial origin, a potential unifying patho-mechanism consistent with vascular dysfunction in DME may converge on cellular senescence. Cells that have entered a state of senescence remain viable and metabolically active yet generate a broad secretome of inflammatory factors and metalloproteases. This state is termed the senescence-associated secretory phenotype (SASP), and modifies the proximal cellular environment and extracellular matrix[17] (reviewed in ref. 18). Senescent endothelial cells (ECs) within the central nervous system lose cell junction integrity and contribute to the breakdown of the BRB[19]. While classically associated with aging, we have previously demonstrated that in vascular units of the retina, cellular senescence can be triggered by environmental stressors independent of age[20–22].

With evidence that senescent cells accumulate in diabetes[20,23–26], and more specifically in the diabetic retina[20–22,27], we sought to investigate the fundamental mechanisms by which senescent cells contribute to DME. We also explored the therapeutic merit of senolysis (elimination of senescent cells) by running a multicenter phase 1 clinical trial with UBX1325 (currently developed as foselutoclax). UBX1325 is a senolytic small molecule that specifically targets senescent cells by inhibiting the antiapoptotic B cell lymphoma-2 (BCL-2)[28] family member BCL-xL.

Results

Pathways of cellular senescence are triggered in the diabetic retina

To determine if cellular senescence contributes to edematous phenotypes observed in patients with DME, we first evaluated levels of prototypical SASP factors in the vitreous of 11 patients with active DME (Supplementary Table 1). Multiplex assessment revealed a significant 1.4-fold increase in plasminogen activator inhibitor 1 (PAI1) and 2-fold increases in levels of interleukin (IL)-6 and IL-8 in patients with active DME when compared to control patients with nonvascular pathology (Fig. 1a). These findings were corroborated with expression of the senescence-associated cell cycle regulator $p16^{INK4A}$ by immunofluorescence in postmortem human retinal sagittal sections of patients with prior diagnosis of DME (65.8 ± 9.7 years of age) when compared to sex-matched and age-matched (71.6 ± 19.2 years of age) nondiabetic control retinas (Supplementary Table 2). We observed elevated expression of $p16^{INK4A}$ in the inner retina (area of active disease), Bruch's membrane and choroidal layers in retinas with DME (Fig. 1b). Expression of $p16^{INK4A}$ was confined to areas of suspected disease activity in patients with DME and was similar to what we reported for patients with PDR[22] and consistent with the presence of SASP factors in the vitreous of patients with diabetes[29]. In addition, PAI1 was expressed in the inner retina in proximity to collagen 4 (COL4)-positive ECs (Fig. 1c).

Pathways of cellular senescence are activated in ECs in the diabetic retina

We next analyzed transcriptomic datasets from bulk RNA sequencing (RNA-seq) of retinas from rats and mice that had streptozotocin (STZ)-induced diabetes for 3 and 2 months, respectively[30]. In STZ-induced diabetes, retinal blood vessels lose barrier function, but animals do not progress to a proliferative disease. In both species, gene-set enrichment analysis (GSEA) revealed a positive correlation in genes for processes of cellular senescence and the SASP in STZ-treated animals compared to citrate-injected controls (Global_Senescence_Literature_Curated_2020; rat normalized enrichment score (NES) = 1.72 with false discovery rate statistical value (FDRq) = 0.01 and mouse NES = 1.29 with FDRq = 0.07; SASP_Literature_Curated_UP; rat NES = 1.57 with FDRq = 0.05 and mouse NES = 1.54 with FDRq = 0.02; Fig. 1d).

To identify retinal cell populations that become senescent in diabetes, we heightened resolution and assessed single-cell (sc)RNA-seq datasets from mice that had STZ-induced diabetes for 25 weeks[31]. We performed principal component analysis and uniform manifold approximation and projection (UMAP) for dimension reduction, which allowed clustering of retinal cell types with similar transcriptional

Fig. 1 | Pathways of cellular senescence are triggered in the diabetic retina. a, Bar charts showing protein levels of SASP factors PAI1, IL-6 and IL-8 (mean ± s.e.m.) in vitreous of humans with DME ($n = 10$) or control ($n = 13–14$). $^*P < 0.05$; $^{***}P < 0.001$ compared to CTR using Student's t-test. **b**, Representative immunostaining illustrating higher levels of $p16^{INK4a}$ in the human DME retinas. Nuclei were counterstained with DAPI. Bar charts represent the quantification of the percentage of $p16^{INK4a}$-positive cells (±s.e.m.) across layers of the human eye in control (CTR; $n = 27$) and DME ($n = 8$) patients. GCL, ganglion cell layer; INL, inner nuclear layer; ONL, outer nuclear layer; RPE, retinal pigment epithelium. $^{**}P < 0.01$ compared to CTR using Student's t-test. **c**, Top, representative immunostaining of PAI1 in retina of control individuals and patients with DME. Blood vessels were stained with COL4 ($n = 3$ retina per group). Bottom, magnified views to show detail. Nuclei were counterstained with DAPI. **d**, GSEA using gene sets Global_Senescence_Literature_Curated_2020 and SASP_Literature_Curated_Up, comparing STZ-induced diabetic rat retinas to nondiabetic control retinas (upper; GSE20886) and STZ-induced diabetic mouse retinas to nondiabetic control retinas (lower; GSE211583). **e**, UMAP representation of integrated retinal cell clusters from nondiabetic and STZ-induced diabetic mouse retina (GSE178121). **f**, Bar chart showing ranked scores, obtained via the Augur pipeline, identifying the most transcriptionally affected cell types in the diabetic retina when compared to control retinas. **g**, Volcano plot showing differential gene expression in ECs of diabetic (STZ) mice compared to controls (absolute $\log_2$ fold change > 0.25, P value < 0.01). **h**, UMAP representation of different subclusters in ECs (GSE178121). **i**, Bar charts showing the distribution (%) of the indicated EC subclusters EC1, EC2 and EC3 among the control and diabetic (STZ) mouse retina. The dot plot depicts the top ten gene markers differentiating EC subclusters based on scRNA-seq data using SCTransform from nondiabetic and STZ-induced diabetic mouse retina. **j**–**l**, Heat maps showing the $\log_2$ fold change in GSVA scores for pathways of cellular senescence (**j**), tight junctions (**k**) and endothelial barrier (**l**) among EC subclusters in STZ retina. **m**, Top, schematic representation of experimental paradigms of radiation-induced senescence (SnC). Senescence of HRMECs was triggered by irradiation (10 Gy, 2 min 45 sec) after 5 to 6 d; transendothelial resistance was then evaluated with ECIS at 4,000 Hz. Bottom, representative images of HRMEC monolayers at increasing concentrations of senescent cells (SnC). Cells were visualized by actin filament staining with phalloidin. **n**, Representative experiment measuring transendothelial resistance (ohm cm^2) using ECIS with increasing percentages of SnC HRMECs. **o**, Bar chart showing transendothelial resistance ($n = 6$ biological replicates), analyzed as the AUC and normalized (mean ± s.e.m., fold of increase) to healthy non-irradiated HRMEC controls (0% SnC). $^{***}P < 0.001$ compared to 0% SnC (control) using one-way analysis of variance (ANOVA).

https://doi.org/10.1038/s41591-024-02802-4

profiles, and identified expected cell populations such as neurons, glial cells and vascular cells (Fig. 1e). To determine the most transcriptionally perturbed retinal cell populations in diabetes, we used the Augur pipeline to assess the performance of a random forest model to differentiate retinal cells in STZ-treated animals from citrate control mice. We found that the top three most affected cell types (highest area

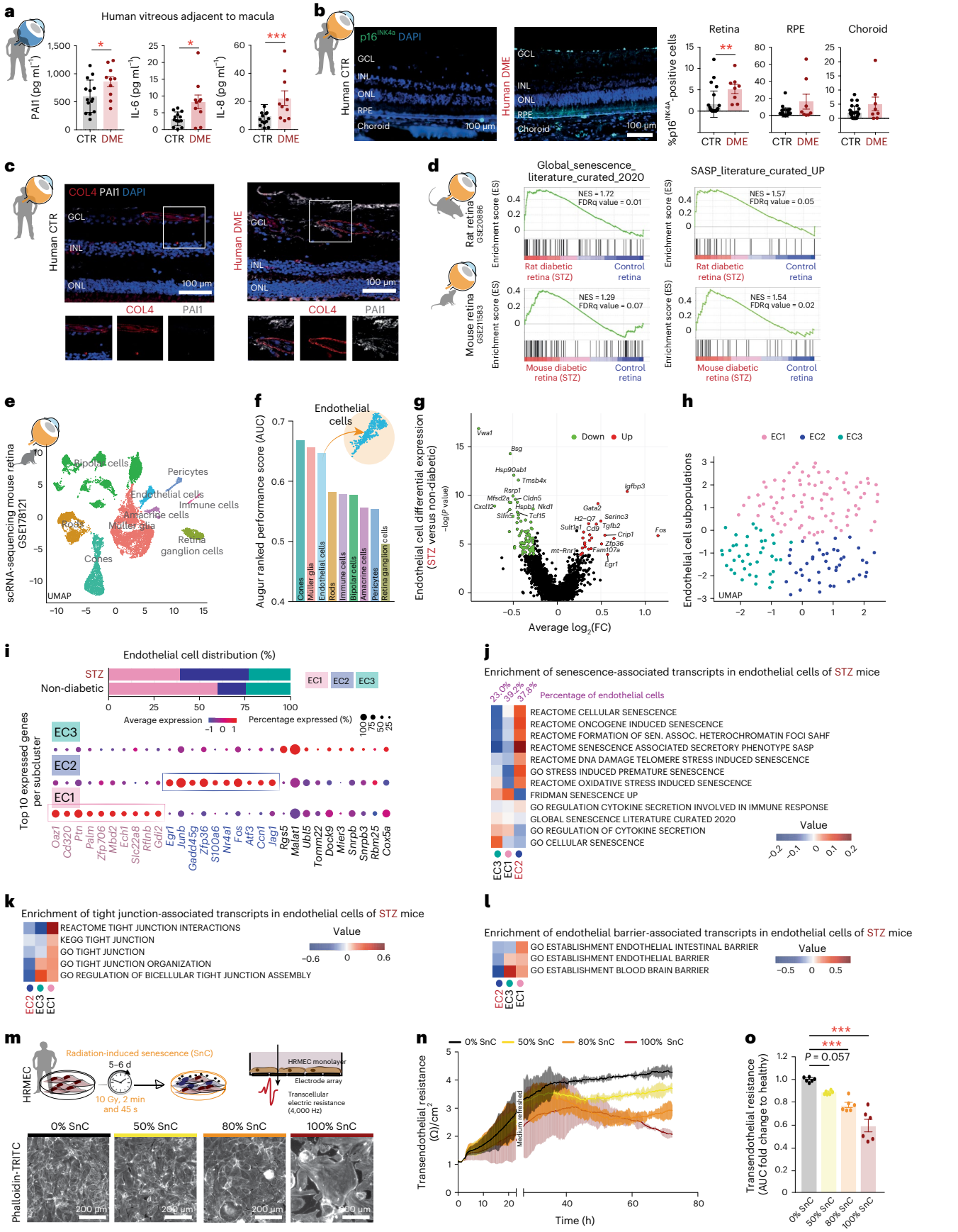

under the curve (AUC)), when compared to nondiabetic control, were cone photoreceptors (score = 0.668), Müller glia (score = 0.656) and ECs (score = 0.647; Fig. 1f).

Because vascular leakage is a pathognomonic feature of DME, we focused on vascular ECs and investigated their transcriptional heterogeneity (Fig. 1g). Principal component analysis and UMAP-based subclustering of ECs revealed three distinct subcellular clusters (EC1, EC2 and EC3) based on their differential gene expression (Fig. 1h). Cluster EC1 (pink) was predominant in nondiabetic retinas (59.6% in nondiabetic versus 39.2% in STZ), whereas cluster EC2 was predominant in the diabetic retinas (blue; 16% in nondiabetic versus 38.8% in STZ). Cluster EC3 (green; 24.4% in nondiabetic versus 23% in STZ) showed equal distribution between diabetic and control groups (Fig. 1i). We then sought to determine the ten most highly expressed genes in each distinct cluster (Fig. 1i). The EC2 cluster, which was elevated in retinas from STZ mice, showed an enrichment for genes that have been previously linked to vascular complications in diabetes, such as *Jag1* (refs. 32,33), *Atf3* (ref. 34), *Egr1* (ref. 35), *Nr4a1* (ref. 36), *Ccn1* (refs. 37,38) and *Junb*[38]. Interestingly, other most expressed genes in EC2, such as *Egr1* (ref. 39), *Gadd45g*[40] and *S100a6* (ref. 29), were previously reported to regulate cellular senescence in ECs and in other cell types[41,42]. Finally, we performed gene-set variation analysis (GSVA) for gene sets related to cellular senescence on EC subclusters from STZ-treated mice. Within diabetic retinas, GSVA positioned the EC2 cluster as the most enriched for senescence-associated genes (Fig. 1j). The gene set encoding for 'Fridman_Senescence_Up', which we previously found to be upregulated in ECs during pathological retinal neovascularization[21,22], was not enriched in the EC2 cluster, suggesting different transcriptomic profiles between senescent ECs in diabetes, and those found in pathological retinal angiogenesis.

Interestingly, and consistent with the pathogenesis of diabetic eye disease, the EC2 cluster also showed the lowest enrichment in genes encoding the biological pathways related to tight junctions (Fig. 1k) and endothelial barrier function (Fig. 1l). Collectively, these data suggest that retinas of STZ-treated mice are enriched in subsets of ECs that express senescence-related transcripts.

EC senescence contributes to loss of barrier function

To assess the outcome of senescent EC burden on barrier function experimentally, we utilized a model of radiation-induced senescence to trigger a uniform DNA damage-induced premature senescence in EC monolayers. We used human retina microvascular ECs (HRMECs) and monitored transendothelial electrical resistance (TEER) while increasing the concentration of senescent cells (SnC; 0%, 50%, 80% mixed with healthy HRMECs; Fig. 1m). In all three conditions (0%, 50% and 80% SnC), a monolayer was achieved after 2 d of incubation. Cultures with 100% SnC served as positive controls, as they did not establish uniform monolayers (Fig. 1m). TEER was determined using an electric cell-substrate impedance sensor (ECIS) measuring cellular resistance in real time at 4,000 Hz to assess barrier function. Compared to control HRMEC cultures with 0% SnC, we observed a decrease in transendothelial resistance as the percentage of senescent cells increased (Fig. 1n,o). As expected, a culture of 100% SnC showed the lowest transendothelial resistance as no uniform monolayer was formed. Altogether, these results support the observation that senescent ECs in the retina compromise barrier function.

Sustained hyperglycemia induces EC senescence and compromises transendothelial junctions

To determine if hyperglycemia can trigger phenotypes of cellular senescence in DME, we exposed HRMEC to a medium with high (25 mM) D-glucose (HG) or isosmotic control enantiomer (CTR; 5 mM D-glucose + 20 mM L-glucose; Fig. 2a). After 5 weeks of exposure to HG[43], global cellular proliferation within each dish was significantly decreased by 25% when compared to cells cultured in CTR (Fig. 2a,b). The reduction in cellular proliferation was accompanied by an increase in cells stained for senescence-associated β-galactosidase (SA-β-gal) activity (6.29% ± 1.41% positive cells in HG; 0.13% ± 0.03% positive cells in CTR; Fig. 2c) and an approximate threefold increase in cells with senescence-associated markers such as accumulation of nuclear promyelocytic leukemia protein (PML) bodies (Fig. 2d) and γH2AX (Fig. 2e) in HG-treated HRMECs compared to CTR.

Sustained exposure to hyperglycemia led to upregulation of $p16^{INK4A}$, p21 and p53 proteins (Fig. 2f). These findings were corroborated with an observed induction in transcripts for cyclin-dependent kinase inhibitors *CDKN1A* and *CDKN2A/INK4A* (Fig. 2g). In addition, the SASP factor PAI1 (SERPINE1) was more abundant in both HRMECs and their supernatants when cultured in HG (Fig. 2h). mRNA levels of the SASP factors *SERPINE1*, *IL6*, *IL8*, *TNF* and ER-stress pathway inositol-requiring enzyme 1α (*ERN1* gene) confirmed these findings (Fig. 2i). Consistent with profiles of cellular senescence, we observed induction of antiapoptotic proteins BCL-2 and BCL-xL in HG-cultured HRMECs (Fig. 2j). These data suggest that sustained hyperglycemia can trigger cellular senescence in cultured primary retinal ECs.

Fig. 2 | Sustained high glucose triggers DNA damage and cellular senescence in ECs. a, Schematic representation of experimental design, where HRMECs are cultured in high-glucose (HG; 25 mM D-glucose). Osmotic control (CTR): 5 mM D-glucose + 20 mM L-glucose (seven independent experiments; scale bar, 100 µm. **b**, Bar chart showing proliferation of HRMECs cultured under HG or CTR condition assessed via reduced Alamar Blue (mean ± s.e.m.; fold change to CTR; $n = 12$ per group over three replicates). ***$P < 0.001$ by Student's *t*-test. **c**, Representative images of cells stained with SA-β-gal are expressed as a percentage of positive cells (blue; ±s.e.m.), $n = 9$ CTR and $n = 12$ HG biological replicates over three experiments. Scale bar, 100 µm. **d**, Left, bar chart showing the number of PML bodies/cell in HRMECs (mean ± s.e.m.; $n = 584$ cells in CTR and $n = 644$ cells in HG, analyzed over three replicates). Right, representative images of one cell nucleus (DAPI) with PML bodies (green). Scale bar, 5 µm. ***$P < 0.001$ by Student's *t*-test. **e**, Representative immunoblots and quantification of γH2AX (mean ± s.e.m.; fold change) in HRMEC lysates ($n = 9$ in CTR and $n = 10$ in HG biological replicates). *$P < 0.05$ using Student's *t*-test. **f**, Representative immunoblots and quantification (mean ± s.e.m.; fold change) of cell cycle arrest proteins p21, p53 and $p16^{INK4A}$ in HRMEC lysates ($n = 5$–11 biological replicates). β-Actin was used as the loading control. *$P < 0.05$ by Student's *t*-test. **g**, Bar charts of RT–qPCR for gene expression (mean ± s.e.m.; fold change) of cell cycle arrest markers *CDKNA1* and *CDKNA2/INK4A* ($n = 13$–17 biological replicates per group) in HRMEC lysates. **$P < 0.01$; ***$P < 0.001$ using Student's *t*-test. **h**, Representative immunoblots and quantification (mean ± s.e.m.; fold change) of SASP-related proteins PAI1 in HRMEC lysates ($n = 9$ or 10 biological replicates per group) and secreted PAI1 in HRMEC supernatant ($n = 6$ biological replicates). β-Actin or Red Ponceau staining served as a loading control. *$P < 0.05$; **$P < 0.01$ using Student's *t*-test. **i**, Bar charts of RT–qPCR for senescence-related gene expression (mean ± s.e.m.; fold change) of *IL6*, *IL8*, *SERPINE1*, *TNF* and *ERN1* ($n = 14$–17 biological replicates per group) in HRMEC lysates. *$P < 0.05$; ***$P < 0.001$ using Student's *t*-test. **j**, Representative immunoblots and quantification (mean ± s.e.m.; fold change) of BCL-2 and BCL-xL in HRMEC lysates ($N = 11$ or 12 biological replicates per group). β-Actin served as a loading control. *$P < 0.05$; **$P < 0.01$ using Student's *t*-test. **k**, Representative immunoblots and quantification of OCLN in HRMEC lysates ($n = 6$ biological replicates per group). β-Actin served as a loading control. *$P < 0.05$ using Student's *t*-test. **l**, Representative immunoblots and quantification (mean ± s.e.m.; fold change) of HRMEC lysates ($n = 6$ biological replicates per group) showing increased Tyr685 phosphorylation of VE-cadherin after conditions of high glucose. β-Actin served as a loading control. *$P < 0.05$ using Student's *t*-test. **m**, Representative immunofluorescence images for VE-cad (in red) and β-cat (in green) in HRMECs cultured under high glucose or control conditions, showing increased internalization of both proteins in HG-treated HRMECs, and especially in cells with senescence-like morphology (indicated with an asterisk). **n**, Quantification of internalized VE-cad and β-cat (mean; fold change to CTR; $n = 121$ cells per group over three replicates). ***$P < 0.001$ using Student's *t*-test.

https://doi.org/10.1038/s41591-024-02802-4

Maintenance of transendothelial junctions requires functional occludin (OCLN)[44,45], vascular endothelial-cadherin (VE-cad) and catenins[46]. HRMECs rendered senescent through exposure to HG for 5 weeks displayed significant reduction in levels of OCLN protein compared to CTR (Fig. 2k), while levels of OCLN mRNA remained unaltered (Supplementary Fig. 1a). In addition, phosphorylation of

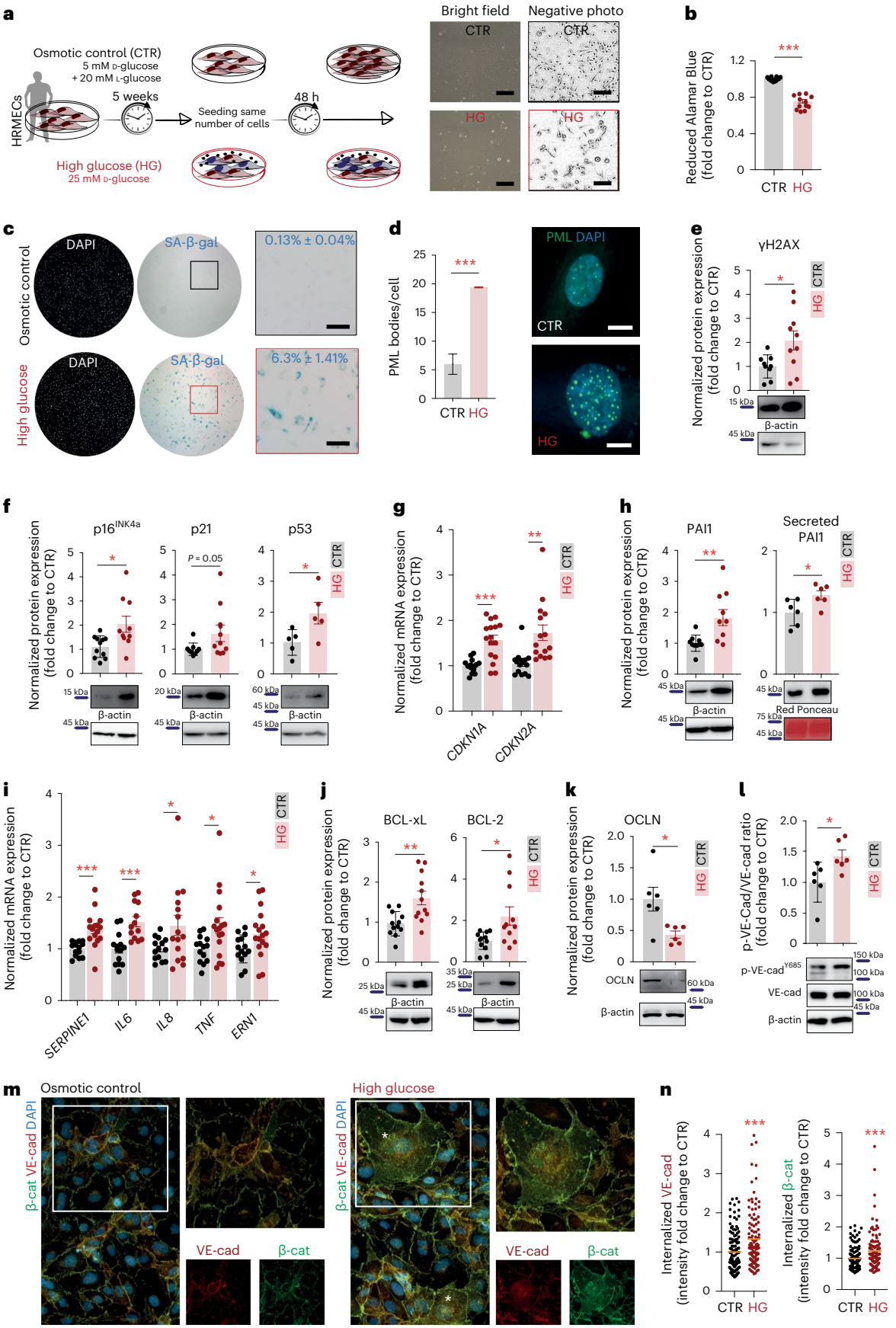

VE-cad on Tyr685 is required for VEGF-A-induced, histamine-induced and bradykinin-induced vascular permeability[47]. Induction of cellular senescence in HRMECs led to heighted phosphorylation of Tyr685 on VE-cad (Fig. 2l) also without affecting transcript levels (Supplementary Fig. 1b). Compromise of transendothelial junctions was visualized using immunofluorescence through the internalization of VE-cadherin/β-catenin in monolayer cultures of HRMECs. Cells subjected to HG revealed ~1.3-fold higher rates of internalization from the plasma membrane to the cytosol of both VE-cad and β-catenin compared to the CTR (Fig. 2m,n).

Senolysis through BCL-xL inhibition improves retinal barrier function in diabetic mice

Consistent with induction of endothelial cellular senescence in the diabetic retina (Fig. 1) and sustained hyperglycemia driving EC senescence (Fig. 2), we observed elevated expression of BCL-xL associated with isolectin B_4 (IB_4)-positive ECs as well as nonvascular cells in retinas of STZ-treated diabetic mice compared to controls (Fig. 3a). BCL-2 expression did not readily colocalize with IB_4, suggesting predominantly extravascular expression (Fig. 3b).

BCL-2 family proteins are critical for the survival of senescent cells[48] and can be targeted to provoke senolysis[22,48–52] through apoptosis (Supplementary Figs. 2a,b and 3a–c). To determine if targeting BCL-xL could ameliorate barrier function in retinas of diabetic mice, we intravitreally administered UBX1967, a small-molecule inhibitor for which we have previously shown dose-dependent (pmol) inhibition of the BCL-xL–BIM interaction in the mouse[22] (Fig. 3c). STZ-treated mice were triaged based on electroretinography (ERG) function with those showing compromised scores randomized for investigation of vascular leakage. Intravitreal injection of either 2 pmol or 20 pmol of UBX1967 at 8 and 9 weeks after STZ administration significantly reduced retinal protein levels of PAI1 and BCL-xL at 10 weeks of diabetes. Retinal BCL-2 remained unchanged (Fig. 3d). Moreover, intravitreal administration of UBX1967 leads to a significant reduction in transcripts for inflammatory SASP factors *Il1b*, *Il6* and *Tnf* as assessed by quantitative PCR with reverse transcription (RT–qPCR; Fig. 3e).

Importantly, intravitreal treatment with UBX1967 led to a robust ~40% to 50% reduction in retinal vascular permeability, as assessed by Evans Blue permeation (EBP) at both doses tested when compared to vehicle diabetic controls (Fig. 3f,g). The propensity of UBX1967 to reduce BRB breakdown was further corroborated by immunostaining of retinal sagittal sections with lower levels of albumin extravasation in perfused animals, observed after treatment with UBX1967 (Fig. 3h).

To investigate if the improvement in retinal barrier function secondary to treatment with UBX1967 leads to enhanced retinal function, we conducted whole-field scotopic ERG. Both scotopic a-wave (relative to photoreceptor function) and b-wave (indicative of inner retina and bipolar cell function) responses were reduced by ~2-fold and ~1.8-fold, respectively, in the diabetic retina (STZ with vehicle) compared to non-diabetic control mice (Fig. 3i,j). Diabetic animals treated intravitreally with UBX1967 at either dose had their a-wave amplitudes augmented by ~1.7-fold with respect to the diabetic vehicle (Fig. 3i), and their scotopic b-wave amplitudes augmented by ~1.5-fold (Fig. 3j), indicating an overall major preservation of electrical activity of the retinal in diabetic mice (Fig. 3i,j). Taken together, inhibition of BCL-xL with UBX1967 improved BRB and retinal function, suggesting a potential therapeutic benefit for senolytic agents in treating diabetic retinal disease.

Results of a single intravitreal injection of UBX1325 in DME patients

We next developed UBX1325, a small-molecule BCL-xL inhibitor with senolytic properties as a therapeutic candidate. UBX1325 and UBX1967 share a common mechanism of action through BCL-xL inhibition, yet UBX1325 is a phosphate pro-drug with improved aqueous solubility that releases the active parent molecule UBX0601 (Fig. 4a). UBX0601 prevented the formation of the antiapoptotic protein complexes through binding of BCL-xL and BCL-2 in biochemical competition binding assays, with inhibitory affinity (pK_i) values greater than $pK_i = 8.6$ (Fig. 4a and Supplementary Table 3). Cellular potency was assessed in MCF-7 human breast cancer cells. After 3 h of incubation with MCF-7 cells, UBX0601 demonstrated potent target engagement (TE) through inhibition of the BCL-xL and BIM interaction (Fig. 4a and Supplementary Table 3). As cellular TE studies indicated that UBX0601 does not engage BCL-2 in MCF-7 cells, we assessed the potential for BCL-2 TE in the healthy mouse retina with UBX1325. At dose levels that provide significant BCL-xL engagement, no evidence of TE at BCL-2 was observed (Fig. 4b).

We then used HRMECs exposed to ionizing radiation to confirm the activity of UBX1325 in a senescent disease-relevant primary cell population as we have done previously[22]. BCL-xL TE in senescent HRMECs was confirmed for UBX0601 after a 2-h incubation ($pIC_{50} = 8.1$), with potencies like those determined in the MCF-7 cell line (Fig. 4c and Supplementary Table 3). To understand the functional consequence of BCL-xL inhibition or mechanism engagement (ME), we monitored a key step in the initiation of apoptosis, activation of caspase-3 and caspase-7. Incubation of a pro-luminescent caspase-3/7 substrate and stabilized luciferase with cell lysate results in a signal indicative of caspase activity. Following a 2-h incubation of UBX0601 with senescent HRMECs, we observed a concentration-dependent increase in caspase activity ($pEC_{50} = 7.3$), which resulted in potencies consistent with BCL-xL TE (Fig. 4c and Supplementary Table 3).

We characterized TE and ME in the diseased retina using the mouse oxygen-induced retinopathy (OIR) model[53] in which we have characterized a heavy burden of senescent cells[20–22]. Consistent with our in vitro and normal healthy retina data, TE in the OIR retina or in normoxic controls showed a potent, dose-dependent inhibition of the BCL-xL–BIM interaction 24 h following injection of UBX1325

Fig. 3 | Targeted elimination of senescent cells reduces diabetes-induced vascular leakage and preserves retinal function. a,**b**, Representative confocal images of flat-mount retinas of nondiabetic control and diabetic STZ retinas. Immunofluorescence for BCL-xL (**a**) and BCL-2 (**b**). BCL-xL was robustly expressed in diabetic retinas and colocalized with ECs (IB_4; representative of four independent retinas per group). **c**, Schematic representation of intravitreal administration schedule of UBX1967. **d**, Representative immunoblots of retinal lysates for PAI1, BCL-2 and BCL-xL after administration of UBX1967 (suspension formulation (20 pmol)). β-Actin served as a loading control (five independent mouse retinas per group). **e**, Bar charts for RT–qPCR showing expression (mean ± s.e.m.; fold change) of SASP-related genes *Il1b* (each *n* is a distinct animal; $n = 8$ for nondiabetic, $n = 9$ for diabetic vehicle, $n = 9$ for diabetic UBX1967 2 pmol, $n = 9$ for UBX1967 20 pmol), *Il6* and *Tnf* (each *n* is a distinct animal; $n = 8$ for nondiabetic, $n = 9$ for diabetic vehicle, $n = 8$ for diabetic UBX1967 2 pmol, $n = 8$ for UBX1967 20 pmol) in mouse retinas after administration of UBX1967 (solution formulation). $^*P < 0.05$; $^{**}P < 0.01$; $^{***}P < 0.001$ using one-way ANOVA. **f**, Schematic representation of the use of Evans Blue (EB; 45 mg per kg body weight) for measuring vascular permeability in the mouse retina during diabetes. **g**, Bar charts showing levels of permeated albumin (mean ± s.e.m.) quantified using the retinal EBP assay ($n = 8$ nondiabetic, $n = 6$ diabetic vehicle, $n = 6$ diabetic UBX1967 2 pmol, $n = 7$ UBX1967 20 pmol independent pools of three mouse retinas) after administration of UBX1967 suspension formulation. $^*P < 0.05$ using one-way ANOVA. **h**, Representative immunostaining illustrating the presence of albumin (ALB) outside blood vessels (IB_4^+) in the diabetic mouse retina after administration of UBX1967 suspension formulation. Nuclei were counterstained with DAPI. Scale bar, 100 µm. Bar chart shows the fold change of extravasated albumin (ALB^+; IB_4^-; $n = 6$ nondiabetic, $n = 8$ diabetic vehicle and $n = 6$ diabetic UBX1967 20 pmol (three independent experiments)). $^{**}P < 0.01$ using a one-way ANOVA. **i**,**j**, Graphs showing the scotopic a-wave (**i**) and b-wave (**j**) responses after treatment with UBX1967, using scotopic ERG ($n = 10$ nondiabetic, $n = 9$ diabetic vehicle, $n = 7$ diabetic UBX1967 2 pmol, $n = 8$ UBX1967 20 pmol independent mice). $^{***}P < 0.001$ and $^*P < 0.05$ using two-way ANOVA.

https://doi.org/10.1038/s41591-024-02802-4

(10–100 pmol; inhibition range, 36–82%; Fig. 4d). However, we only observed caspase-3/7 activity in OIR retinas, but not in normoxic controls (Fig. 4e). Together, these data suggest that initiation of apoptosis through inhibition of BCL-xL requires the presence of senescent cells, and that apoptosis does not occur with BCL-xL inhibition in a healthy retina (Fig. 4e). We then assessed vascular leakage in the STZ model and

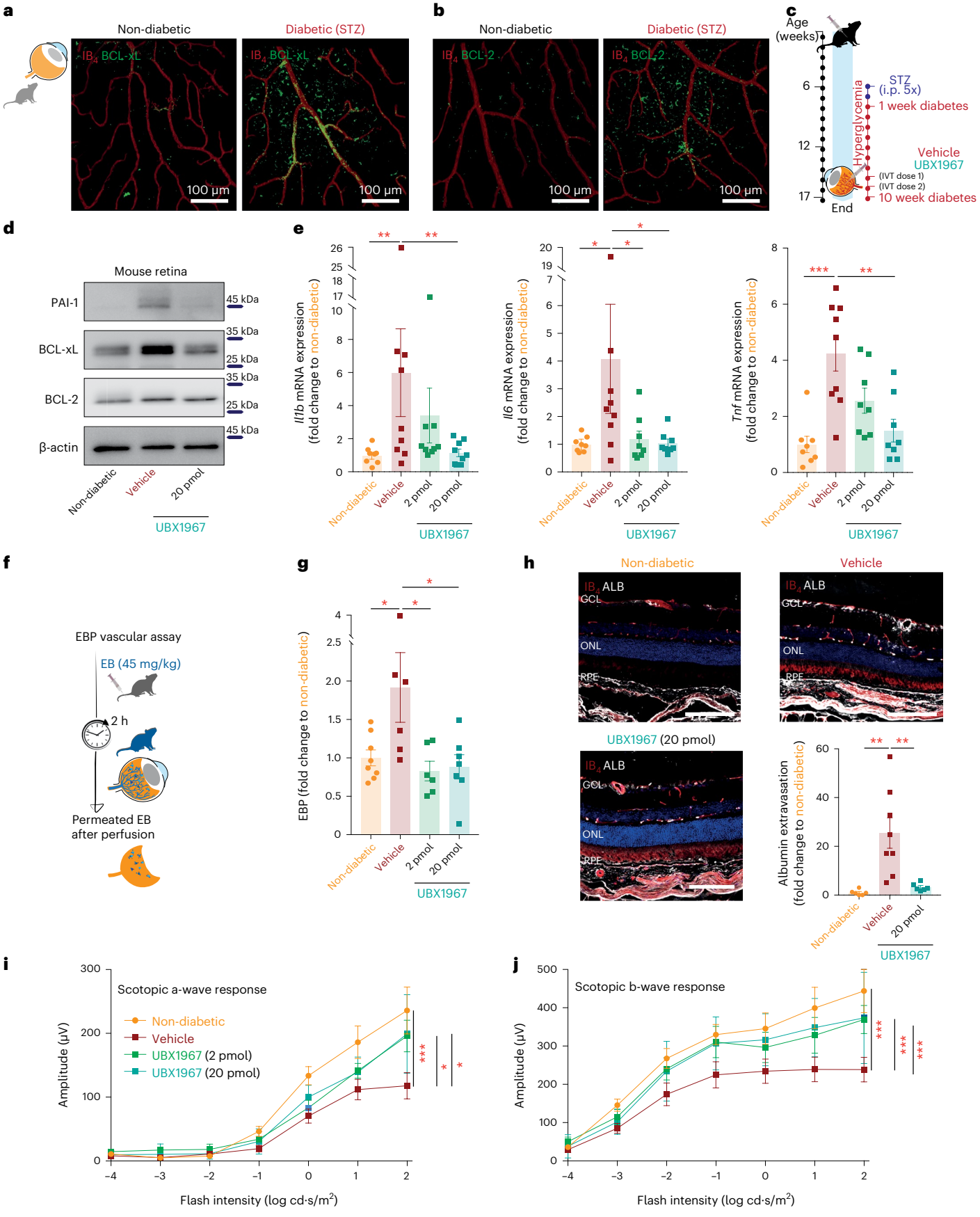

https://doi.org/10.1038/s41591-024-02802-4

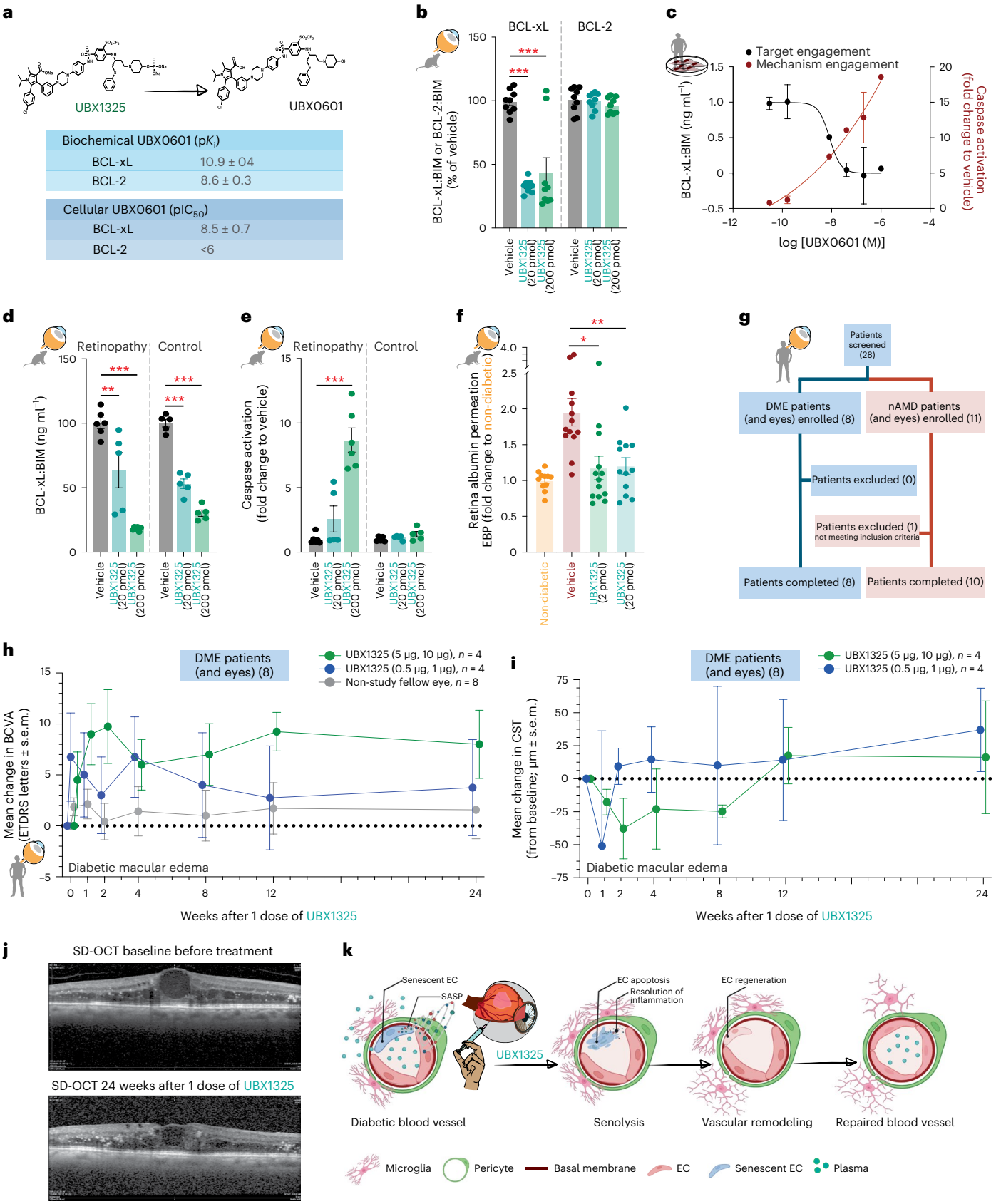

observed that, similarly to UBX1967 (Fig. 3f), intravitreal treatment with UBX1325 significantly reduced retinal vascular permeability by ~40% to 50% when compared to vehicle-treated diabetic controls (Fig. 4f).

We conducted a 24-week phase 1 single ascending dose (SAD) safety and tolerability study of UBX1325 in patients with advanced disease from DME for whom anti-VEGF therapy was no longer considered beneficial by their treating physician (Fig. 4g, Table 1 and Extended Data Table 1). In addition, patients with a different retinal vascular disease (neovascular AMD (nAMD)) were also included in the phase 1 safety trial (Fig. 4g). In these latter patients, their treating physician

https://doi.org/10.1038/s41591-024-02802-4

Fig. 4 | Intravitreal injection of UBX1325 in patients with DME. a, Top, chemical structures of UBX1325 and its active derivative, UBX0601. Bottom, values represent in vitro biochemical affinity (pK_i) values and cellular potency (pIC_{50} in MCF-7) for UBX0601 toward BCL-xL and BCL-2. **b**, Comparison of retinal TE of UBX1325 for BCL-xL and BCL-2 in the adult mouse retina ($n = 9$ independent animals per group). Data are expressed as a percentage (±s.e.m.) of either BCL-xL–BIM or BCL-2–BIM complexes to vehicle-injected mice. ***$P < 0.001$ using one-way ANOVA. **c**, Graph showing BCL-xL–BIM complexes (left axis) and caspase-3/7 activation (right axis) detected 2 h after incubation of senescent HRMECs with UBX0601. BCL-xL–BIM complex data are expressed as the fraction of BCL-xL–BIM normalized to controls. Caspase-3/7 activation is expressed as fold change over DMSO vehicle control ($n = 118$ over 11 replicates). **d**, Retinal TE for BCL-xL at postnatal day (P)13 after intravitreal injection of UBX1325 at P12 in mouse with OIR or control normoxic littermates. Data are expressed as a percentage (±s.e.m.) BCL-xL–BIM complexes compared to vehicle-injected mice ($n = 6$ vehicle, $n = 5$ UBX1325 20 pmol and $n = 6$ UBX1325 200 pmol independent retinas with retinopathy and $n = 5$ vehicle, $n = 5$ UBX1325 20 pmol and $n = 5$ UBX1325 200 pmol independent retinas control). **$P < 0.01$; ***$P < 0.001$ using one-way ANOVA. **e**, Caspase-3/7 activity in the retina on P13 after intravitreal injection at P12 of UBX1325 in mouse with OIR or control normoxic littermates. Data are expressed as the fold change (mean ± s.e.m.) relative to vehicle-injected animals ($n = 6$ vehicle, $n = 5$ UBX1325 20 pmol and $n = 6$ UBX1325 200 pmol independent retinas with retinopathy and $n = 5$ vehicle, $n = 5$ UBX1325 20 pmol and $n = 5$ UBX1325 200 pmol independent retinas control). ***$P < 0.001$ using one-way ANOVA. **f**, Bar charts showing levels of extravasated albumin quantified using the EBP assay in the retina ($n = 11$ nondiabetic, $n = 13$ diabetic vehicle, $n = 13$ diabetic UBX1325 2 pmol and $n = 12$ UBX1325 20 pmol (n of 1 contains 3 mouse retinas). *$P < 0.05$, *$P < 0.01$ using one-way ANOVA. **g**, Patient flow diagram for the clinical trial. Patients with DME ($n = 8$) received a single intravitreal injection of UBX1325 following assessment of BCVA (**h**) and CST (**i**) (mean ± s.e.m.) up to 24 weeks. Data on CST include the study eye only because a central reading was not used for SD-OCT in the fellow eye. **j**, Representative SD-OCT imaging of a patient who showed a decrease of 108 µm of CST and an increase of 11 ETDRS letters over the 24-week period of the trial. **k**, Schematic representation of the senescence disease hypothesis in DME: senescent ECs accumulate in retinal blood vessels during diabetes and contribute to elevation of retinal micro-inflammation and BRB breakdown, ultimately leading to reduced visual function. Inhibition of BCL-xL with the small-molecule inhibitor UBX1325 selectively eliminates senescent cells and leads to vascular repair. Created in part with BioRender.com.

Table 1 | Baseline characteristics of patients with DME

	Low dose (*N*=4)	High dose (*N*=4)
	Mean (±s.d.)*	Mean (±s.d.)*
Age (years)	71.8 (±6.45)*	66.0 (±9.38)*
BMI (kg/m^2)	35.5 (±9.93)*	36.7 (±10.18)*
Sex (male:female)	3:1	0:4
BCVA (ETDRS letters, study eye)	25.0 (±18.62)*	46.5 (±10.66)*
BCVA (ETDRS letters, non-study eye)	57.0 (±15.38)*	76.8 (±13.00)*
CST (µm)	792 (±464)*	540 (±154)*
DRSS score (minimum, maximum, *n*)	43 (43, 43, 2)	35 (35, 35, 4)

BMI, body mass index.

Table 2 | Summary of ocular TEAEs by severity for all patients with DME and nAMD

	UBX1325						
No. of events (%)	0.5 µg (*N*=3)	1.0 µg (*N*=3)	5.0 µg (*N*=3)	10.0 µg (*N*=10)	Low dose (*N*=6)	High dose (*N*=13)	Overall (*N*=19)
Patients with at least one TEAE	0	2 (66.7)	0	10 (100)	2 (33.3)	10 (76.9)	12 (63.2)
Related TEAE	0	0	0	0	0	0	0
Grade ≥3 TEAE	0	0	0	2 (20.0)	0	2 (15.4)	2 (10.5)
Serious TEAE	0	0	0	1 (10.0)	0	1 (7.7)	1 (5.3)
Ocular TEAE for study eye	0	1 (33.3)	0	9 (90.0)	1 (16.7)	9 (69.2)	10 (52.6)
Treatment-related ocular TEAE for study eye	0	0	0	0	0	0	0
DLT-defining adverse event	0	0	0	0	0	0	0
TEAE leading to death	0	0	0	0	0	0	0

also determined that they would not benefit from ongoing treatment with anti-VEGF therapy in their study eye. In both diseases, the study eye was chosen as the most affected eye. The primary outcome of the trial was safety and tolerability with efficacy being exploratory.

UBX1325 was delivered by intravitreal injection and was well tolerated at all doses tested (through 10 µg) without dose-limiting toxicities (DLTs) and no reported incidence of inflammation. There were few non-ocular treatment-emergent adverse events (TEAEs), all of which were considered unrelated to UBX1325 by both the treating investigator and the Safety Monitoring Committee for the study. Ocular TEAEs were all deemed mild to moderate and were all either unrelated or unlikely related to UBX1325 (Table 2 and Supplementary Table 4). While there were numerically more reports of TEAEs in those patients receiving the higher doses of UBX1325, all were considered due to the patients' underlying retinal disease. IOP was measured for all patients following UBX1325 injection and then on all subsequent visits. A single patient receiving 1 µg UBX1325 had an IOP of ≥25 mm Hg, representing an increase of ≥10 mm Hg from baseline. For this patient, the IOP returned to normal before discharge from the clinic (within hours) and had no other elevation in IOP throughout the remainder of the study. Other than this patient, there were no IOP measurements in any patient, in study or fellow eye, that exceeded 25 mm Hg nor more than 10 mm Hg change from baseline (Supplementary Table 4). Assessment of TEAEs, IOP, clinical observation and imaging modalities led to the conclusion that UBX1325 was well tolerated in these patients. Initial safety assessment confirmed that UBX1325 could be advanced into later-stage clinical studies, including in patients with less severe forms of DME or nAMD.

For all analyzed patients, plasma concentrations of UBX1325 and its active parent molecule (UBX0601) were below the lower limit of quantification (100 pg ml^{-1} and 20 pg ml^{-1}, respectively) at 0.5, 1, 2, 4 and 24 h after a single intravitreal injection of UBX1325 at doses up to 10 µg in all 18 participants who were enrolled with DME or nAMD and completed day 1 pharmacokinetic sampling. Based on the SAD study, no measurable systemic exposures of UBX1325 or UBX0601 would be expected at doses up to 10 µg after a single intravitreal injection.

Among patients with DME enrolled in the study ($n = 8$), a single injection of UBX1325 led to an improvement in visual acuity: in 6 of 8 patients at 12 weeks, and in 5 of 8 patients at 24 weeks. In higher-dose cohorts (5, 10 µg), patients had a mean improvement of 9.5 ± 4.4 (mean ± s.e.m.) Early Treatment Diabetic Retinopathy Study (ETDRS) letters from baseline at 24 weeks (Fig. 4h and Supplementary Table 5). Among all DME patients, 62.5% showed a gain of 5 or more letters at 24 weeks, and 50% had gained 10 or more letters at 24 weeks (Supplementary Table 5).

Consistent with preclinical data (Fig. 3), higher doses of UBX1325 reduced central subfield thickness (CST), with most patients remaining stable through 24 weeks (Fig. 4i) as observed through spectral domain-optical coherence tomography (SD-OCT; Fig. 4j). Among patients with DME, diabetic retinopathy severity scale (DRSS) scores

were evaluable in six patients and did not change in any patient. In evaluable patients, four receiving 5 or 10 µg had baseline scores of 35 (mild NPDR) and two receiving 1 µg had a baseline score of 43 (moderate NPDR). Patients with nAMD saw lesser increases in best-corrected visual acuity (BCVA) and movement of CST in the weeks following administration than patients with DME, with measures returning to those observed in the fellow, non-study eye by 4 weeks (Supplementary Fig. 4a,b).

Discussion

The conceptual framework for clearance of senescent cells to improve aging-associated disorders had been proposed over a decade ago[54]. Here we provide clinical evidence supporting this idea by demonstrating that therapeutic clearance of senescent cells can lead to long-term improvements in visual function in patients with DME. Non-laser-based therapeutic interventions to control DME have largely centered on VEGF-A or broad targeting of inflammation with nonspecific corticosteroids[5]. While effective, these treatments address late-stage patho-mechanisms, and are not efficacious for a significant portion of patients[55]. In addition, they require frequent, repeated intravitreal injections to maintain efficacy. We describe a mechanism within retinal vasculature where sustained hyperglycemia triggers molecular pathways that are commonly associated with organismal aging and culminate in cellular senescence. Senescent vascular ECs display lower expression of tight junction occludins and higher levels of internalized transendothelial junction proteins such as VE-cadherin, and hence are inefficient at maintaining BRB function. Intravitreal administration of a small-molecule inhibitor of BCL-xL eliminates senescent ECs leading to reduced local inflammation and regeneration of a vascular unit with improved barrier function (Fig. 4k). Ultimately, visual function is improved.

Repeated monthly or bimonthly intravitreal injections have become common practice in ophthalmology yet reducing injection frequency would improve quality of life for patients and decrease cost to healthcare systems. Recently, intravitreal injection intervals have been increased up to 16 weeks with the approval of high-concentration formulations[56,57]. The efficacy of these drugs, as with most biologics, is driven by their vitreous/retinal residency time and once they leave the eye, another injection is required. In contrast, the mode of action of senolytic drugs such as UBX1325 or UBX1967 is driven by their ability to rapidly engage mechanism of action and eliminate damaged cells[22], and not their vitreous/retinal residency. While the senescence disease hypothesis needs to be tested in larger cohorts, our exploratory phase 1 efficacy data suggest that improvements in vision last at least 6 months. In addition, our results in mice reveal that BCL-xL inhibition eliminates disease-causing senescent cells thereby reducing micro-inflammation, modifying the retinal microenvironment and ultimately re-establishing tissue homeostasis. Taken with previous data in a mouse model of preretinal neovascularization[22], inhibition of BCL-xL may provide broad benefit across vascular diseases of the retina. Hence, therapeutic clearance of senescent cells can potentially remove an underlying source of pathogenesis and thus allow healthy ECs to regenerate and remodel retinal vasculature, ultimately leading to long-term disease modification.

Our data also highlight the influence of different stressors on the kinetics and penetrance of induction of cellular senescence. Cellular senescence following exposure to high glucose has previously been reported in cultures with short-term exposure[58–61]. However, in accordance with others[43], we observe that ECs require protracted exposure to sustained high glucose (>5 weeks) to trigger cellular senescence and that senescence only occurs in subsets of hyperglycemia-exposed cells. In contrast, stimuli such as oxidative stress[20] or hyperactivation of the RAS pathway, as seen in pathological angiogenesis[21], rapidly provoke EC senescence within less than a week[21]. The requirement for prolonged hyperglycemia is likely an adaptive mechanism to protect from natural postprandial spikes in glycemia. While future trials will shed light on the duration of effect of senolytics, retinal complications from diabetes typically manifest after 10 to 20 years of disease[62,63] and hence treatment with UBX1325 has the potential to lead to long-lasting disease modification. Barrier function in the retina is mediated by tight interplay of several cell populations including vascular ECs, pericytes, astrocytes, Müller cells, microglia and neurons[64]. While the current study focused on the role of ECs in BRB integrity, we have observed enrichment in transcripts encoding pathways of cellular senescence in non-EC populations in a different model of retinal vasculopathy[22]. It is plausible that these senescent components of the neurovascular unit also contribute to vascular leakage in DME, and their targeting with UBX compounds may be part of a comprehensive disease-modifying mechanism.

Collectively, our data identify senolysis through BCL-xL inhibition with UBX1325 as a potential long-lasting therapeutic approach to promote vascular repair and remodeling within the diabetic retina. More broadly, given that accretion of senescent cells has been observed in multiple geriatric and metabolic diseases, senolytic drugs may have the potential to become aspirational treatments for a spectrum of age-relate conditions.

Online content

Any methods, additional references, Nature Portfolio reporting summaries, source data, extended data, supplementary information, acknowledgements, peer review information; details of author contributions and competing interests; and statements of data and code availability are available at https://doi.org/10.1038/s41591-024-02802-4.

References

1. Antonetti, D. A., Klein, R. & Gardner, T. W. Diabetic retinopathy. *N. Engl. J. Med.* **366**, 1227–1239 (2012).
2. Levine, S. R., Sapieha, P., Dutta, S., Sun, J. K. & Gardner, T. W. It is time for a moonshot to find "Cures" for diabetic retinal disease. *Prog. Retin. Eye Res.* **90**, 101051 (2022).
3. Stitt, A. W. et al. The progress in understanding and treatment of diabetic retinopathy. *Prog. Retin. Eye Res.* **51**, 156–186 (2016).
4. Yu, D. Y. et al. Retinal capillary perfusion: spatial and temporal heterogeneity. *Prog. Retin. Eye Res.* **70**, 23–54 (2019).
5. Duh, E. J., Sun, J. K. & Stitt, A. W. Diabetic retinopathy: current understanding, mechanisms, and treatment strategies. *JCI Insight* **2**, e93751 (2017).
6. Heier, J. S. et al. Intravitreal aflibercept for diabetic macular edema: 148-week results from the VISTA and VIVID studies. *Ophthalmology* **123**, 2376–2385 (2016).
7. Scott, A. W., Bressler, N. M., Ffolkes, S., Wittenborn, J. S. & Jorkasky, J. Public attitudes about eye and vision health. *JAMA Ophthalmol.* **134**, 1111–1118 (2016).
8. Bressler, N. M. et al. Persistent macular thickening following intravitreous aflibercept, bevacizumab, or ranibizumab for central-involved diabetic macular edema with vision impairment: a secondary analysis of a randomized clinical trial. *JAMA Ophthalmol.* **136**, 257–269 (2018).
9. Rofagha, S. et al. Seven-year outcomes in ranibizumab-treated patients in ANCHOR, MARINA, and HORIZON: a multicenter cohort study (SEVEN-UP). *Ophthalmology* **120**, 2292–2299 (2013).
10. Comparison of Age-related Macular Degeneration Treatments Trials Research Group. et al. Five-year outcomes with anti-vascular endothelial growth factor treatment of neovascular age-related macular degeneration: the comparison of age-related macular degeneration treatments trials. *Ophthalmology* **123**, 1751–1761 (2016).
11. Robinson, G. S. et al. Nonvascular role for VEGF: VEGFR-1, 2 activity is critical for neural retinal development. *FASEB J.* **15**, 1215–1217 (2001).

12. Kurihara, T., Westenskow, P. D., Bravo, S., Aguilar, E. & Friedlander, M. Targeted deletion of Vegfa in adult mice induces vision loss. *J. Clin. Invest.* **122**, 4213–4217 (2012).
13. Berber, P., Grassmann, F., Kiel, C. & Weber, B. H. An eye on age-related macular degeneration: the role of microRNAs in disease pathology. *Mol. Diagn. Ther.* **21**, 31–43 (2017).
14. Saint-Geniez, M. et al. Endogenous VEGF is required for visual function: evidence for a survival role on Müller cells and photoreceptors. *PLoS ONE* **3**, e3554 (2008).
15. Jones, R. 3rd & Rhee, D. J. Corticosteroid-induced ocular hypertension and glaucoma: a brief review and update of the literature. *Curr. Opin. Ophthalmol.* **17**, 163–167 (2006).
16. Little, H. L. Treatment of proliferative diabetic retinopathy. Long-term results of argon laser photocoagulation. *Ophthalmology* **92**, 279–283 (1985).
17. Coppe, J. P. et al. Senescence-associated secretory phenotypes reveal cell-nonautonomous functions of oncogenic RAS and the p53 tumor suppressor. *PLoS Biol.* **6**, 2853–2868 (2008).
18. Coppé, J. -P., Desprez, P. -Y., Krtolica, A. & Campisi, J. The senescence-associated secretory phenotype: the dark side of tumor suppression. *Annu. Rev. Pathol.* **5**, 99–118 (2010).
19. Yamazaki, Y. et al. Vascular cell senescence contributes to blood–brain barrier breakdown. *Stroke* **47**, 1068–1077 (2016).
20. Oubaha, M. et al. Senescence-associated secretory phenotype contributes to pathological angiogenesis in retinopathy. *Sci. Transl. Med.* **8**, 362ra144 (2016).
21. Binet, F. et al. Neutrophil extracellular traps target senescent vasculature for tissue remodeling in retinopathy. *Science* **369**, eaay5356 (2020).
22. Crespo-Garcia, S. et al. Pathological angiogenesis in retinopathy engages cellular senescence and is amenable to therapeutic elimination via BCL-xL inhibition. *Cell Metab.* **33**, 818–832 (2021).
23. Palmer, A. K. et al. Cellular senescence in type 2 diabetes: a therapeutic opportunity. *Diabetes* **64**, 2289–2298 (2015).
24. Thompson, P. J. et al. Targeted elimination of senescent beta cells prevents type 1 diabetes. *Cell Metab.* **29**, 1045–1060 (2019).
25. Aguayo-Mazzucato, C. et al. Acceleration of beta cell aging determines diabetes and senolysis improves disease outcomes. *Cell Metab.* **30**, 129–142 (2019).
26. Su, L. et al. Diabetic endothelial cells differentiated from patient iPSCs show dysregulated glycine homeostasis and senescence associated phenotypes. *Front. Cell Dev. Biol.* **9**, 667252 (2021).
27. Lamoke, F. et al. Increased oxidative and nitrative stress accelerates aging of the retinal vasculature in the diabetic retina. *PLoS ONE* **10**, e0139664 (2015).
28. Singh, R., Letai, A. & Sarosiek, K. Regulation of apoptosis in health and disease: the balancing act of BCL-2 family proteins. *Nat. Rev. Mol. Cell Biol.* **20**, 175–193 (2019).
29. Bao, L. et al. The S100A6 calcium-binding protein regulates endothelial cell-cycle progression and senescence. *FEBS J.* **279**, 4576–4588 (2012).
30. VanGuilder, H. D. et al. Multi-modal proteomic analysis of retinal protein expression alterations in a rat model of diabetic retinopathy. *PLoS ONE* **6**, e16271 (2011).
31. Sun, L. et al. Single cell RNA sequencing (scRNA-seq) deciphering pathological alterations in streptozotocin-induced diabetic retinas. *Exp. Eye Res.* **210**, 108718 (2021).
32. Miloudi, K. et al. NOTCH1 signaling induces pathological vascular permeability in diabetic retinopathy. *Proc. Natl Acad. Sci. USA* **116**, 4538–4547 (2019).
33. Yoon, C. H. et al. Diabetes-induced Jagged1 overexpression in endothelial cells causes retinal capillary regression in a murine model of diabetes mellitus: insights into diabetic retinopathy. *Circulation* **134**, 233–247 (2016).
34. Okamoto, A., Iwamoto, Y. & Maru, Y. Oxidative stress-responsive transcription factor ATF3 potentially mediates diabetic angiopathy. *Mol. Cell. Biol.* **26**, 1087–1097 (2006).
35. Karthikkeyan, G. et al. Hyperglycemia induced early growth response-1 regulates vascular dysfunction in human retinal endothelial cells. *Microvasc. Res.* **117**, 37–43 (2018).
36. Venu, V. K. P. et al. Metformin prevents hyperglycemia-associated, oxidative stress-induced vascular endothelial dysfunction: essential role for the orphan nuclear receptor human nuclear receptor 4A1 (Nur77). *Mol. Pharmacol.* **100**, 428–455 (2021).
37. Li, H. et al. Diabetes promotes retinal vascular endothelial cell injury by inducing CCN1 expression. *Front. Cardiovasc. Med.* **8**, 689318 (2021).
38. You, J. J., Yang, C. M., Chen, M. S. & Yang, C. H. Regulation of Cyr61/CCN1 expression by hypoxia through cooperation of c-Jun/AP-1 and HIF-1alpha in retinal vascular endothelial cells. *Exp. Eye Res.* **91**, 825–836 (2010).
39. Ao, H., Liu, B., Li, H. & Lu, L. Egr1 mediates retinal vascular dysfunction in diabetes mellitus via promoting p53 transcription. *J. Cell. Mol. Med.* **23**, 3345–3356 (2019).
40. Bruemmer, D. et al. Regulation of the growth arrest and DNA damage-inducible gene 45 (GADD45) by peroxisome proliferator-activated receptor gamma in vascular smooth muscle cells. *Circ. Res.* **93**, e38–e47 (2003).
41. Hoare, M. et al. NOTCH1 mediates a switch between two distinct secretomes during senescence. *Nat. Cell Biol.* **18**, 979–992 (2016).
42. Passegue, E. & Wagner, E. F. JunB suppresses cell proliferation by transcriptional activation of $p16^{INK4a}$ expression. *EMBO J.* **19**, 2969–2979 (2000).
43. Bertelli, P. M. et al. Long term high glucose exposure induces premature senescence in retinal endothelial cells. *Front. Physiol.* **13**, 929118 (2022).
44. Murakami, T., Felinski, E. A. & Antonetti, D. A. Occludin phosphorylation and ubiquitination regulate tight junction trafficking and vascular endothelial growth factor-induced permeability. *J. Biol. Chem.* **284**, 21036–21046 (2009).
45. Murakami, T., Frey, T., Lin, C. & Antonetti, D. A. Protein kinase cbeta phosphorylates occludin regulating tight junction trafficking in vascular endothelial growth factor-induced permeability in vivo. *Diabetes* **61**, 1573–1583 (2012).
46. Huber, A. H. et al. The cadherin cytoplasmic domain is unstructured in the absence of beta-catenin. A possible mechanism for regulating cadherin turnover. *J. Biol. Chem.* **276**, 12301–12309 (2001).
47. Claesson-Welsh, L., Dejana, E. & McDonald, D. M. Permeability of the endothelial barrier: identifying and reconciling controversies. *Trends Mol. Med.* **27**, 314–331 (2021).
48. Zhu, Y. et al. Identification of a novel senolytic agent, navitoclax, targeting the Bcl-2 family of anti-apoptotic factors. *Aging Cell* **15**, 428–435 (2016).
49. Zhu, Y. et al. The Achilles' heel of senescent cells: from transcriptome to senolytic drugs. *Aging Cell* **14**, 644–658 (2015).
50. Gonzalez-Gualda, E., Baker, A. G., Fruk, L. & Munoz-Espin, D. A guide to assessing cellular senescence in vitro and in vivo. *FEBS J.* **288**, 56–80 (2021).
51. Chang, J. et al. Clearance of senescent cells by ABT263 rejuvenates aged hematopoietic stem cells in mice. *Nat. Med.* **22**, 78–83 (2016).
52. Yosef, R. et al. Directed elimination of senescent cells by inhibition of BCL-W and BCL-XL. *Nat. Commun.* **7**, 11190 (2016).
53. Smith, L. E. et al. Oxygen-induced retinopathy in the mouse. *Invest. Ophthalmol. Vis. Sci.* **35**, 101–111 (1994).
54. Baker, D. J. et al. Clearance of p16Ink4a-positive senescent cells delays ageing-associated disorders. *Nature* **479**, 232–236 (2011).

55. Gonzalez, V. H. et al. Early and long-term responses to anti-vascular endothelial growth factor therapy in diabetic macular edema: analysis of protocol I data. *Am. J. Ophthalmol.* **172**, 72–79 (2016).
56. Wykoff, C. C. et al. Pharmacokinetics of the port delivery system with ranibizumab in the Ladder phase 2 trial for neovascular age-related macular degeneration. *Ophthalmol. Ther.* **11**, 1705–1717 (2022).
57. Faricimab (Vabysmo) for age-related macular degeneration and diabetic macular edema. *Med. Lett. Drugs Ther.* **64**, 45-46 (2022).
58. Abouhish, H. et al. Inhibition of HDAC6 attenuates diabetes-induced retinal redox imbalance and microangiopathy. *Antioxidants* **9**, 599 (2020).
59. Gericke, A., Suminska-Jasinska, K. & Breborowicz, A. Sulodexide reduces glucose induced senescence in human retinal endothelial cells. *Sci. Rep.* **11**, 11532 (2021).
60. Mortuza, R., Feng, B. & Chakrabarti, S. miR-195 regulates SIRT1-mediated changes in diabetic retinopathy. *Diabetologia* **57**, 1037–1046 (2014).
61. Thounaojam, M. C. et al. MicroRNA-34a (miR-34a) mediates retinal endothelial cell premature senescence through mitochondrial dysfunction and loss of antioxidant activities. *Antioxidants* **8**, 328 (2019).
62. Diabetes, C. et al. The effect of intensive treatment of diabetes on the development and progression of long-term complications in insulin-dependent diabetes mellitus. *N. Engl. J. Med.* **329**, 977–986 (1993).
63. Nentwich, M. M. & Ulbig, M. W. Diabetische retinopathie. *Der Diabetol.* **6**, 491–502 (2010).
64. Antonetti, D. A., Silva, P. S. & Stitt, A. W. Current understanding of the molecular and cellular pathology of diabetic retinopathy. *Nat. Rev. Endocrinol.* **17**, 195–206 (2021).

[1]Department of Biochemistry, Maisonneuve-Rosemont Hospital Research Centre, University of Montreal, Montreal, Quebec, Canada. [2]Department of Ophthalmology, Centre Universitaire d'Ophtalmologie (CUO-HMR) Maisonneuve-Rosemont Hospital Research Centre, University of Montreal, Montreal, Quebec, Canada. [3]UNITY Biotechnology, South San Francisco, CA, USA. [4]Departments of Pediatrics Ophthalmology, and Pharmacology, Centre Hospitalier Universitaire Sainte Justine Research Center, Montreal, Quebec, Canada. [5]Department of Medicine, Maisonneuve-Rosemont Hospital Research Centre, University of Montreal, Montreal, Quebec, Canada. [6]Present address: École d'optométrie, University of Montreal, Montreal, Quebec, Canada. ✉e-mail: mike.sapieha@umontreal.ca

Methods

Human vitrectomy study design and analysis

All human studies adhered to the Declaration of Helsinki. Studies using vitreous biopsy samples from patients were approved by the Ethical Committee at the Hospital Maisonneuve-Rosemont. Histological ocular tissue was purchased at different providers, and appropriate consent or authorization regarding the use and distribution of the samples according to the pertinent regulations was obtained.

Patients with DME were enrolled in the study and severity was determined using optical coherence tomography (OCT). Patients with CST ≥ 350 µm with subretinal or intraretinal fluid and no vitreomacular traction were considered to have center-involved DME. Control patients included in the study underwent pars plana vitrectomy for diseases of the vitreomacular interface (for example, epiretinal membrane, macular hole) and did not have a history of ocular inflammation or previous vitrectomy or diabetes. Patients with DME were subjected to a partial vitreous biopsy. The same surgeon collected all vitreous samples including control patients with nonvascular pathology and DME patients (before intravitreal injection during scheduled treatment) at the Hospital Maisonneuve-Rosemont (Montreal, Canada). Undiluted core and cortical vitreous samples adjacent to the macular region were extracted. Vitreous was preserved immediately in dry ice and later stored at −80 °C. Protein levels were analyzed by protein multiplex assays following the manufacturer's indications: Milliplex Map Kit HCYTOMAG-60K (Millipore) to detect IL-6 and IL-8 and Milliplex Map Kit HADCYMAG-61K (Millipore) to detect PAI1. Information relative to the patient and vitreous samples is in Supplementary Table 1.

Human eye histological studies

Histological ocular tissue used to detect $p16^{INK4A}$ was purchased at the Kansas Eye Bank, the San Diego Eye Bank, the National Development and Research Institute or the Human Eye Biobank for Research at St. Michael's Hospital. Ocular tissue (whole eye including the optic nerve and lens) was collected from the eye bank and received at Excalibur Pathology. Fixation was done by injecting 0.5 ml Davidson's fixative near the limbus and followed by immersion with Davidson's fixative for 48–72 h. After that, samples were placed in 70% ethanol and later embedded in paraffin blocks by Excalibur Pathology. Histological ocular tissue used to detect the rest of the targets was purchased at the Lion's Gift of Sight eye bank. No information regarding the collection or fixation of the tissues was available, and samples were provided already cut on glass slides.

All patients were diagnosed with DME using the patient history, and nondiabetic controls were matched for age and sex. Information available relative to the patient and vitreous samples is in Supplementary Table 2. Sagittal paraffin sections of ~4 µm were deparaffinized and rehydrated before immunolabeling. $p16^{INK4A}$ (Supplementary Table 3) was detected as previously described[22] using CINTec (Roche) and a diethylaminocoumarin DCC fluorochrome assay on the Ventana Discovery Platform (Roche). Nuclei were counterstained with DAPI. Slides were scanned using an Axioscan microscope (Zeiss) and the number of $p16^{INK4A}$-positive cells was quantified using image analysis software (Visiopharm) and relativized to total DAPI-positive cells. COL4 and PAI1 were detected using the antibodies listed in Supplementary Table 6 in tissue subjected to citrate buffer (pH 6) antigen retrieval. Samples were blocked in 3% BSA and incubated with the antibodies overnight. Signal was detected using species-appropriate fluorochrome-conjugated secondary antibodies, and nuclei were counterstained with DAPI. Slides were visualized using an Olympus FV1000 laser scanning confocal microscope. Quantification was performed in a masked manner.

Animal study design and experimental models

All animal experimentation was previously approved by local ethical authorities at the Hospital Maisonneuve-Rosemont (CPA protocol 2019-1877), at UNITY Biotechnology or at the Vanderbilt Ocular (VO)-CRO hired by UNITY Biotechnology. Animal experiments also adhered to the ARRIVE guidelines and to the ARVO statement for the use of animals in ophthalmic and vision research. Male and female C57BL/6J mice were purchased from the Jackson Laboratories. *CD1* lactating mothers were purchased from Charles River. All animals were housed in 12-h cycle of light and darkness with free access to chow and water. Animals tested negative for the RD8 mutation[65].

OIR was carried out as described previously[22,32]. In brief, C57BL/6J pups, both males and females, and their corresponding fostering mothers (CD1 female) were exposed to 75% O_2 from P7 to P12 and returned to room air afterwards. This model resembles an ischemic insult that leads to cellular senescence in the retina and that we have previously characterized in depth[22]. All mice were housed in 12-h–12-h light–dark cycles, at 23–25 °C and a relative humidity (around 50%) in ventilated cages.

Low-dose STZ (Sigma-Aldrich) was resuspended in 10 mM sodium citrate buffer (pH 4.5) and injected intraperitoneally at a concentration of 55 mg per kg body weight during five consecutive days. Only C57BL/6J males were enrolled in the study at the age of 6 weeks, and were randomly assigned to the multiple experimental groups. Blood glycemia and weight were monitored before and after induction of diabetes, and then weekly during the time course of the experiment up to 10 weeks after diabetes induction. Animals were considered diabetic when fasting blood glucose levels were >17 mM (starting 1 week after the last injection). Control mice were injected with vehicle. Before treatment, animals were triaged using scotopic ERG at 8 weeks of diabetes to assess compromise of visual function due to diabetes.

Intravitreal injections in mouse models

UBX1967 was synthesized by UNITY Biotechnology or a partner organization (Ascentage Pharma). UBX1325 and UBX0601 were synthesized by UNITY Biotechnology. Formulation development was conducted by UNITY Biotechnology. We investigated the mechanism of action of the experimental BCL-2 family inhibitors, UBX1967 and UBX1325 (UNITY Biotechnology), in interventional studies using C57BL/6J mice in the models of STZ-induced diabetes and OIR. Both UBX1967 and UBX1325 selectively target senescent cells expressing members of the BCL-2 family, and trigger apoptosis for tissue clearance. In OIR, pups were injected intravitreally at P12 using a 10-µl syringe (Hamilton) with a glass capillary coupled onto it. Each treated pup had both eyes injected with either 1 µl of UBX1325 or 1 µl of appropriate vehicle control. Vehicle formulation was 1% DMSO, 1% polysorbate (PS)-80, 20% polyethylene glycol (PEG)-400 (in PBS) for administration of UBX1967 and 0.3% PS-80 (in PBS) for administration of UBX1325.

In STZ-induced diabetes, animals were evaluated at different time points depending on the experiment. Animals were anesthetized superficially with isoflurane, and eyes were kept open using surgical nylon. Volume was loaded in a 10-µl syringe (Hamilton) with a coupled glass capillary. Animals that experienced excessive reflux, bleeding or in which the lens was accidentally pierced were excluded from the study. UBX1967 for ERG and gene expression studies and UBX1325 for EBP studies were performed at the VO-CRO using a solution formulation of UBX1967 in 2.5% PS-80 in PBS or UBX1325 in 0.3% PS-80 in PBS. All other studies were performed at the Hospital Maisonneuve-Rosemont using a suspension formulation of UBX1967 in 1% DMSO, 20% PEG-400 and 1% PS-80 in PBS. Each treated eye was injected intravitreally with 1 µl of UBX1967 at a concentration of either ~2 µM (2 pmol) or ~20 µM (20 pmol).

Whole-retina RNA-seq studies in mouse models

Each RNA-seq replicate was obtained from one single retina of a hyperglycemic mouse 8 weeks after intraperitoneal STZ injection, or citrate-injected control, and was extracted using the RNeasy Mini Kit (Qiagen) and purified from 1 µg of total RNA using the Dynabeads mRNA DIRECT Micro Kit (Thermo Fisher Scientific). Whole-transcriptome libraries were prepared using the Ion Total RNA-seq Kit v2 (Thermo Fisher Scientific). The yield and size distribution of the amplified libraries

were assessed with the Agilent Bioanalyzer using the DNA 1000 Kit. Sequencing was performed on an Ion Proton instrument (Ion Torrent, Thermo Fisher Scientific). Analysis was performed using the Torrent Suite software v5.4.0 (Thermo Fisher Scientific) and the RNA-Seq Analysis plugins (Thermo Fisher Scientific). The RNA-Seq Analysis plugins align reads on the mouse reference genome (mm10) using STAR, and then unmapped reads are aligned using Bowtie2 and merged. Gene-level expression is calculated using HTSeq and Picard to report raw read counts and FPKM (fragment per kilobase of transcript per million). Data have been deposited in the Gene Expression Omnibus under accession number GSE211583. Differential expression analysis was performed with DESeq2 and used for pre-ranked GSEA (v.4.0.3; http://www.broad.mit.edu/gsea/) in: (1) STZ-induced diabetic rat retina lysates (GSE20886)[30] with five control and four STZ retina samples, and (2) STZ-induced diabetic mouse retina lysates (described above) with three control and two STZ retina samples. Enrichment in pathways of cellular senescence was interrogated using the previously published gene sets: Global_senescence_literature_curated_2020 and SASP_literature_curated_UP[21,22].

scRNA-seq studies in mouse models

scRNA-seq analysis on control and STZ-induced diabetic retina cells (GSE178121; with three mouse retina pooled in either one control or one STZ retina samples; animals were diabetic for 25 weeks)[31] was performed with kb-python v0.27.4 (read alignment)[66] and Seurat v5 (dimensionality reduction, cell clustering, differential gene expression analysis)[67] and cell-type-specific transcriptional profiles were used for cell-type prioritization (Augur v1)[68] and pathway enrichment with GSVA (v1.51.1)[69] at the single-cell level, allowing differential analysis of pathway expression between STZ and control retinal cell types. Gene sets used for GSVA were obtained from the Molecular Signature Database[70] or previously published senescence gene sets. Molecular Signature Database was used to fetch specific pathways using keywords (for example, 'SENESCENCE', 'TIGHT JUNCTION' and 'ENDOTHELIAL BARRIER') to produce heat maps of differential pathway expression (log_2FC) between EC subclusters.

In vitro cellular models

Primary HRMECs were purchased from either Cell Systems (ACBRI181) or Neuromics and maintained to a population doubling level of <1 and following the manufacturer's instructions. Cells were maintained in a humidified incubator at 37 °C with 5% CO_2.

MCF-7 cells (American Type Culture Collection) were cultured in Eagle's Minimum Essential Medium (American Type Culture Collection) supplemented with human recombinant insulin (0.01 mg ml^{-1}; Thermo Fisher), 10% FBS (VWR Life Science) and penicillin–streptomycin (1×; Thermo Fisher). Cells were maintained at ~70% confluency in a humidified incubator at 37 °C with 5% CO_2.

Induction of endothelial senescence in vitro

HRMECs from three independent lots were expanded in vitro according to the manufacturer's instructions. To induce glucose-driven senescence, HRMECs were exposed in vitro to hyperglycemic conditions (HG) at 5 mM D-glucose (already in medium) supplemented with +20 mM D-glucose for a period of 5 weeks. Treatment with +20 mM L-glucose served as osmotic control (CTR). Culture media were changed every 48 h and no variations in pH of culture media were detected throughout the course of experiments in any group. Alternatively, cellular senescence was induced via ionizing radiation (4 Gy min^{-1}, or 10–12 Gy total); after 5–6 d, HRMECs showed a senescence-like phenotype and stopped proliferating. In all cases, cells were monitored daily using an inverted microscope and maintained in culture up to passage 10 at 37 °C and 5% CO_2 and medium was refreshed every second day.

Another model of rapid cellular senescence triggered by high glucose was achieved by subjecting the HRMECs to 280 mM D-glucose for 2 weeks (only used in Supplementary Fig. 3). 5 mM D-glucose served as a control.

Visualization of endothelial monolayers in vitro

The different mixes of healthy and irradiated HRMECs were plated on a 0.1% gelatin-coated 96-well tissue culture plate for 24 h at 37 °C with 5% CO_2. Samples were fixed in 4% paraformaldehyde (PFA) for 6 min at room temperature (RT) and then washed twice with PBS for 5 min. Samples were permeabilized in PBS supplemented with Triton X-100 (0.05%) for 10 min at RT followed by two washes with PBS. Samples were then incubated with a mix of phalloidin-TRITC (P1951, Sigma; dilution of 1:1,000) and DAPI (D9542, Sigma; dilution of 1:10,000) for 30 min at RT, and later washed with PBS. For each sample, *z*-stacks were taken on a Zeiss Axio Observer Z1 motorized inverted microscope coupled with an MRm monochrome CCD camera. AxioVision software (Zeiss) was used for image processing and editing.

TEER studies

Replicative stress cellular senescence was elicited using radiation as previously described in Methods (4 Gy min^{-1}, or 10–12 Gy total). After 5–6 d, HRMECs ceased proliferation and adopted a senescence-like morphology. To study the burden of senescence in the endothelial monolayer, we established groups with an ascending percentage of senescent cells (50%, 80% and 100%) mixed with healthy non-irradiated HRMECs (50%, 20% and 0%, respectively). Cultures containing 100% healthy non-irradiated HRMECs (0% senescent) served as negative control. Real-time TEER was measured using an ECIS (Z-Theta; Applied Biophysics) as described elsewhere[32]. In brief, 18,000 cells per well (HRMECs) were plated in 96-well plates (96W10idfPET, Applied Biophysics). This well array has an electrode area of 2.09 mm^2 that can measure a maximum of 2,000–4,000 cells. Firstly, the cells were incubated at RT for 20 min for them to precipitate uniformly before placing the array in the incubator. This led to a homogeneous precipitation of the cells, higher survival and a more rapid formation of the monolayers. Plates were then inserted in a 96-well array station, and impedance was set at 4,000 Hz for TEER measurement. After approximately 24 h, medium was refreshed to eliminate non-adherent cells, and we verified at the inverted microscope the formation of the monolayers across all conditions. Real-time TEER was measured up to 70 h with the ECIS software (v1.2), and TEER resistance (Ω) was relativized to cm^2 and analyzed as the AUC.

Cellular proliferation assays in vitro

Senescence-associated growth arrest was analyzed in vitro with glucose-induced senescence in HRMECs using the Alamar Blue assay (Sigma-Aldrich) following the manufacturer's indications. In short, cells were seeded at a concentration of 10^3 cells per well in a 96-well plate. Twelve hours after, Alamar Blue reactive was added, and proliferation rates were determined at 4 h measuring the oxidation and reduction of the compound by means of absorbance according to the manufacturer's instructions.

Senescence-associated β-gal assay

HRMECs or mouse retinas were fixed with 4% PFA and washed thoroughly with PBS before incubating with a solution containing: 1 mM $MgCl_2$ in PBS (pH 6), 5 mM $K_4Fe(CN)_6$, 5 mM $K_3Fe(CN)_6$ and 5-bromo-4-chloro-3-indolyl β-D-galactoside (X-Gal; Bioshop) solution for ~10 h at 37 °C. Samples were counterstained with DAPI (3 μM) for 5 min. Senescence-associated β-gal signal was imaged in an Axio Observer Z1 microscope (Zeiss). SA-β-gal-stained cells (blue) were quantified using ImageJ (US National Institutes of Health) and normalized to a number of DAPI-stained nuclei.

Evaluation of nuclear PML bodies in ECs

Cells were grown onto coverslips and fixed with 4% PFA, washed with PBS and permeabilized with 0.2% Triton X-100 and 3% BSA for 5–15 min. PML (Supplementary Table 6) was then incubated for 2 h and signal was detected using a fluorochrome-conjugated secondary antibody.

Nuclei were counterstained with DAPI. Samples were visualized using an Axio Observer Z1 (Zeiss) motorized inverted microscope, and PML bodies were quantified using the feature to count foci of Zen v2.3 image acquisition software (Zeiss). A total of 584 cells (CTR) and 644 cells (HG) were evaluated.

Live-cell imaging apoptosis assay

In total, 9,000 cells per well of non-irradiated healthy HRMECs (control group) and 18,000 cells per well of irradiated HRMECs (senescent group) were plated in 96-well plates and allowed to settle for 18 h. The next day, the medium was removed and replaced with 200 µl of refreshed complete medium (EBM2 + EGM2MV) supplemented with 2 µl NucView and 2 µl MitoView (NucView 488 and MitoView 633 Apoptosis Assay Kit, Biotium) in a 1:100 ratio for 30 min at 37 °C and 5% CO_2 in the dark. Cells were then treated with increasing doses of UBX1967 and imaged every 15 min for 24 h using a Zeiss microscope coupled to a controlled chamber (37 °C, 5% CO_2). Analysis and quantification of apoptosis (Supplementary Fig. 2) was performed based on the fluorescence signal captured and following the manufacturer's instructions.

Immunoblotting

Protein expression was evaluated by means of western blot using standard procedures. In brief, mouse retinas (UBX1967 20 pmol in 1% DMSO, 20% PEG-400, 1% PS-80) or HRMECs were lysed using RIPA buffer with protease and phosphatase inhibitors, and 15–20 µg of protein were separated by electrophoresis in 10–12.5% acrylamide gels. Proteins were then transferred to methanol-activated PVDF membranes, blocked in 5% skim milk or 5% BSA TBS solution and incubated with specific antibodies overnight (Supplementary Table 6). Signal was detected using horseradish peroxidase-conjugated species-appropriate secondary antibodies in a Chemiluminescence Imaging System (ImageQuant LAS4000, GE Healthcare Life Sciences). Quantification of the proteins was performed using ImageJ and expressed as fold change over the loading control, housekeeping gene β-actin expression. Ponceau S staining solution was used for qualitative technical assessment. Each unprocessed membrane is linked to the pertinent figure and the bands displayed are indicated.

Gene expression analysis (RT–qPCR) in ECs

HRMECs were washed with PBS and harvested by adding TRIzol using a pipette directly onto the culture plate and immediately snap frozen. HRMEC mRNA was extracted using either a standardized TRIzol reagent (Thermo Fisher) protocol or Direct-zol RNA Micro Prep Kit (Zymo Research). cDNA was prepared using iScript Reverse Transcription Supermix (Bio-Rad). qPCR was performed to quantify gene expression using iTap Universal SYBR Green Supermix (Bio-Rad) in a QuantStudio 7 Flex Applied Biosystems (Life Technologies). Primer sequences are compiled in Supplementary Table 7. *ACTB* gene expression was used as the reference housekeeping gene. Gene expression was analyzed using the ΔΔCt method. Statistical analysis was performed on ΔΔCt values and is represented as the fold change of increase to control.

VE-cadherin internalization studies in vitro

HRMECs were fixed in 4% PFA at RT for 5 min. Fixed HRMECs were blocked with 3% BSA and 0.1% Triton X-100 solution and incubated overnight at 4 °C with antibodies against β-catenin and VE-cadherin (Supplementary Table 6) overnight. Probes were later incubated for 3 h with fluorescence-conjugated species-appropriate secondary antibodies and nuclei counterstained with DAPI. Imaging of random density-matched, unspecific fluorescence-background-matched regions was performed by a blinded experimenter using Zen Blue edition 3.2 software on the Zeiss Axio Imager Z2 microscope). *Z*-stacks with 1-µm steps were processed into optical sections using ApoTome.2 (three phases for image capture) and processed using local bleaching correction and strong Fourier filter features provided by the software. To compare expression levels between images, no intensity normalization was performed. Cells were identified by DAPI staining, and cytosolic β-catenin and VE-cadherin mean fluorescence intensity was determined for each individual cell (n = 118 to 121 cells per condition within two independent experiments) using ImageJ.

Fluorescence immunolabeling of retina whole mounts

Eyes were enucleated and fixed in 4% PFA for 1 h at RT, followed by an overnight incubation with PBS supplemented with 10% sucrose. Eyes were then embedded in optimal cutting temperature medium and cut in sagittal 12-µm sections on a cryostat. After washing, sections were blocked with 1% BSA and incubated with specific antibodies (Supplementary Table 6). Signal was detected using a fluorophore-conjugated species-appropriate secondary antibody and imaged using an Olympus FV1000 confocal microscope. Images were processed using Olympus FluoView software (Olympus).

Gene expression analysis (RT–qPCR) in whole mouse retina

Intravitreal injections were used to deliver 1 µl of UBX1967 (2 pmol or 20 pmol in 2.5% PS-80) and appropriate vehicle. Eye globes were freshly collected after euthanasia and the retinas placed into RNAlater solution. cDNA was prepared using the cDNA Super-Scrip II RT (Invitrogen). Quantitative PCR was run using SYBR Green PCR Master Mix and the indicated probes on a StepOnePlus Real-Time PCR System (Applied Biosystems by Life Technologies). All probes are listed in Supplementary Table 7. *Actb* was used a reference gene, and gene expression was analyzed using the ΔΔCt method.

Evans Blue vascular permeability assay

Intravitreal injections were used to deliver 1 µl of UBX1967 (2 pmol or 20 pmol in 1% DMSO, 20% PEG-400 and 1% PS-80 in PBS), UBX1325 (2 pmol or 20 pmol in 0.3% PS-80 in PBS) or appropriate vehicle (1st dose at week 8, 2nd dose at week 9). Vascular permeability was assessed at week 10 using the colorimetric assay of EBP (Sigma-Aldrich) in 16-week-old diabetic mice. EB was injected at a concentration of 45 mg per kg body weight intravenously in the tail. After circulating for 2 h, mice were anesthetized by isoflurane, and blood plasma was obtained via cardiac puncture and was followed by perfusion with PBS. Eyes were collected and fixed in 4% PFA during 1 h at 4 °C before retina and sclera were dissected. Three retinas were pooled together and incubated in 200 µl formamide overnight at 65 °C. Evans Blue was quantified using a plate reader (Infinite M200 Pro, Tecan Life Sciences; conditions using a maximum absorbance of 620 nm and minimum absorbance of 740 nm). Permeated Evans Blue was normalized to the Evans Blue present in plasma, and to the wet tissue weight. EBP values were calculated as per µl g^{-1} h^{-1} and are expressed as fold change values of the increase to the nondiabetic (citrate) group.

Histological evaluation of vascular permeability in mouse

Intravitreal injections were used to deliver 1 µl of UBX1967 (2 pmol or 20 pmol in 1% DMSO, 20% PEG-400 and 1% PS-80 in PBS) and appropriate vehicle (1st dose at week 8, 2nd dose at week 9). Animals were anesthetized and perfused at week 10 with PBS. Mouse eyes were enucleated, fixed for 2 h in 4% PFA and embedded in OCT compound. Sagittal 10-µm sections (containing at least partly the optic nerve head) were blocked using 3% BSA and subjected to immunodetection of albumin (ALB) and blood vessels (IB_4) (Supplementary Table 6), counterstained with DAPI and systematically imaged using an FV1000 confocal microscope (Olympus). Extravasated albumin was determined as the area positive for albumin and negative for IB_4 in the neuroretina. Quantification was performed in a masked manner using ImageJ, and extravasated albumin is expressed as a percentage in relation to the total neuroretina region.

ERG in mouse studies

Intravitreal injections were used to deliver 1 µl of UBX1967 (2 pmol or 20 pmol in 2.5% PS-80) and appropriate vehicle (1st dose at week 8, 2nd

dose at week 9). Visual function was evaluated at baseline (week 8 of diabetes) and later after treatment (week 10 of diabetes) by means of whole-field ERG. In brief, animals were adapted to darkness overnight and later anesthetized subcutaneously with a cocktail containing ketamine (13.2 mg ml^{-1}) and xylazine (1.5 mg ml^{-1}) at a concentration of 3.7 ml per kg body weight. Eyes were proptosed, and pupils dilated with tropicamide (1%) and moisturized with Genteal eye drops. Animals were kept thermostatically controlled using a rectal temperature feedback probe (37 °C). ERG was recorded using ultralow-impedance silver/nylon DTL Plus fiber electrodes. Needle electrodes were placed on the middle of the forehead (reference) and in the tail (ground). A gold contact lens electrode was used to record ERG responses. Mice were then located under an ERG dome (UTAS-E Visual Electrodiagnostic Test System) and flash ERGs were recorded. Scotopic ERGs were evoked using increasing flashes of light (λ = 500 nm with a maximum intensity of 1,200 mW/cm^2), with an interval of stimuli of 50 ms.

Biochemical and cellular TE of BCL-2 family proteins

Biochemical inhibitory affinity (pK_i) values for UBX0601 (Fig. 4) or UBX1967 (Supplementary Fig. 3) were determined in a biochemical competition assay using purified, His-tagged, BCL-2 and BCL-xL proteins, and biotinylated BIM or BAD peptides, in 25 mM HEPES, 100 mM NaCl, 0.1% BSA and 0.005% PS-80 at a pH of 7.5. Test molecules and peptides were combined before initiation of the assay by the addition of the BCL-2 family protein, followed by incubation at RT overnight. Complexes were detected (Alpha Technology, Perkin Elmer) using anti-6-His AlphaLISA Acceptor Beads and streptavidin AlphaScreen Donor Beads.

Cellular TE for BCL-xL and BCL-2 was determined in MCF-7 cells and senescent HRMECs. UBX0601 was diluted serially and incubated with cells for 2–3 h at 37 °C and 5% CO_2. The assay was terminated by cell lysis in 0.05% PS-20 in PBS. Measurement of BCL-xL–BIM and BCL-2–BIM complexes was determined using the Meso Scale Discovery (MSD) platform. Anti-BCL-2 and anti-BCL-xL (71 ng per well; Supplementary Table 6) were used to capture complexes from cell lysate incubation for 1 h at RT. Plates were washed, and a Sulfo-tagged anti-BIM detection antibody (100 ng; Supplementary Table 6) was added to each well followed by incubation for 1 h at RT. After washing plates, MSD Read Buffer was added and the electrochemiluminescent signal was measured. Data were interpolated from a standard curve of recombinant protein complexes (Novus Biologicals) to determine amounts in pg ml^{-1}. Results are expressed as the fraction response.

Cellular ME of caspase-3 and caspase-7

Senescent HRMECs were incubated with the test molecule as described for TE above, and initiation of apoptosis was determined by activation of caspase-3 and caspase-7. The cell lysate was incubated with Caspase-Glo (Promega) per the manufacturer's instruction. Luminescence signal was normalized to control conditions and expressed as fold induction over control.

Whole-retina target and ME studies

TE for BCL-xL was determined in 8- to 12-week-old C57BL/6J mice (The Jackson Laboratory). Animals were injected (2 µl, intravitreal) with UBX1325 or vehicle, and retinas were harvested 6 h after dose. BCL-xL TE was also determined in OIR and normoxic mice after a single administration of UBX1325. Animals were injected (1 µl, intravitreal) with test molecule or vehicle at P12, and retinas were harvested 24 h after injection for the dose–response studies.

Retinas were homogenized using the Precellys tissue homogenizer (Bertin Instruments) in lysis buffer (1 mM EDTA, 2% CHAPS in PBS). TE was determined on the MSD platform as above but using the anti-BIM antibody for capture and the Sulfo-tagged anti-BCL-xL antibody for detection. Data were interpolated from a standard curve of recombinant protein complexes to determine amounts in pg ml^{-1} and normalized to the vehicle control samples. ME was determined by Caspase-Glo (Promega) per the manufacturer's instructions, and data are expressed as the fold induction over the vehicle controls.

Trial design and oversight

The phase 1 study was an open-label, first-in-human, SAD study consisting of approximately four cohorts. The total number of participants was three per cohort (two patients with DME and one patient with nAMD) and up to an additional seven patients with nAMD enrolled in the highest-dose (10 µg) cohort. A single dose of UBX1325 was administered intravitreally, and all participants were followed for approximately 6 months. The clinical trial protocol (Supplementary Note 1) and STROBE checklist (Supplementary Note 2) are provided.

All participants provided written informed consent before being screened. The participant information sheet detailed the procedures involved in the study (aims, methodology, potential risks and anticipated benefits) and the investigator explained these to each participant. The participant signed the consent form to indicate that the information had been explained and understood. The participant was then allowed time to consider the information presented before signing and dating the informed consent form to indicate that they fully understood the information, and willingly volunteered to participate in the study. The participant was given a copy of the informed consent form for their information. The original copy of the informed consent was kept in a confidential file in the investigator's center records.

The study was performed in compliance with the requirements of the US Food and Drug Administration. The study gained regulatory approval from the Food and Drug Administration on 25 August 2020, conducted under US Investigational New Drug number 145348. The study gained full approval from the central Institutional Review Board Advarra on 6 August 2020.

Oversight for the study was done through a Safety Assessment Committee (SAC) that met to review all safety data following any sentinel dosing and after completion of a dosing cohort. At each meeting, the principal investigators or their designees were available to answer questions and describe any observed findings. Each dose escalation required formal SAC approval.

Trial sites and patient population

The study was conducted at eight clinical sites located within the United States (three in Florida, two in California, two in Texas and one in Indiana). The study enrolled participants with either the diagnosis of DME or with nAMD. An enrolled participant was one who was deemed eligible and who was assigned to a treatment cohort. Approximately 21 DME and nAMD participants were planned to enroll in this study with a total of 19 evaluable participants enrolled.

Among the participants with DME, the major inclusion criteria were: age ≥ 18 years; evidence of NPDR who were, in the opinion of the investigator, inadequately responding to, unlikely to benefit from or had failed current treatment options; presence of center-involved DME with CST ≥ 350 µm on SD-OCT at day 1; BCVA at screening and on day 1 in the study eye of 70 ETDRS letters (approximately equivalent to 20/40 on the Snellen chart) or worse; BCVA in the non-study eye of 35 ETDRS letters (approximately equivalent to 20/200 on the Snellen chart) or better. Determination of the study eye was based on selection of the eye most affected by DME or nAMD. Major exclusion criteria were: concurrent disease in the study eye or structural damage, other than DME or nAMD, that could compromise BCVA or BCVA improvement; HbA1c ≥ 12 and/or recent signs of uncontrolled diabetes; history of vitreous hemorrhage in the study eye within 2 months before screening; concomitant therapy with anti-VEGF therapies or previous use of these agents in the study eye within 90 d of enrollment; use of systemic and intraocular steroid use for 6 months before enrollment, panretinal photocoagulation within 6 months before enrollment or macular laser photocoagulation 3 months before enrollment.

Enrollment, treatments assignments and dose rationale

After a patient was identified as potentially eligible for the study, the patient was invited to participate. If the patient agreed to study participation, written informed consent was obtained before any study-specific procedures were performed. Patients who consented to participate in the study were assigned a screening number. After each eligible participant consented, the site staff obtained a UBX1325 dose assignment and a unique participant number. Following receipt of the participant number and dose assignment, the site staff prepared the study drug as instructed by the pharmacy manual.

The doses administered in the study were 0.5, 1.0, 2.5, 5.0 and 10 µg. The starting dose of 0.5 µg was chosen based on the totality of the data provided by the non-GLP toxicology studies in both New Zealand White rabbits and cynomolgus monkeys and the pharmacologically active dose level in the mouse OIR model. Doses in preclinical species were converted to vitreous maximum concentration (C_{max}) values based on accepted vitreous humor volume estimates in each of the nonclinical species and then scaled to human C_{max} vitreal concentrations of UBX1325. The ratio of the C_{max} at the assigned No Observed Adverse Effect Level in the most sensitive GLP safety species was used to calculate safety margins for all proposed doses in the phase 1 escalation. The starting dose of 0.5 µg in humans was supported by a 29-fold margin in rabbits and a 109-fold margin in the nonhuman primate.

Intervention and dose escalation

Study drug was administered only to patients who signed and dated an informed consent form and were approved for enrollment into the trial. The study drug, UBX1325, was administered by intravitreal injection under aseptic technique in accordance with institutional requirements and best practices. The individual at the site responsible for intravitreal administration was delegated to conduct this activity by the principal investigator and approved by the sponsor and documented as such in the Delegation of Responsibilities Log. Each patient received a single intravitreal injection of a fixed volume of 50 µl of study. All study drug was administered within 1 h of preparation.

Data collection

An electronic data capture system was designed and managed on behalf of the sponsor by the sponsor's designated contract research organization. Clinical data were entered by study site personnel within five business days of the patient visit or activity conduct. Monitoring of the study was conducted on site by a designee of the sponsor who conducted document and source data review, as well as remote data monitoring in the intervals between monitoring visits. Data were reviewed remotely by the medical monitor for safety oversight. All study-related information was recorded on source documents. All required study data were recorded in the electronic case report forms, and data were required to be submitted to the sponsor throughout and at the end of the study in a timely and accurate manner. The data were checked for completeness and correctness in real time online by the sponsor.

Outcome measures

Outcome measures that were assessed at all sites in the study included those evaluating the primary objective of safety and tolerability including anterior and posterior segment evaluation and ophthalmoscopy, IOP, color fundus photography, DRSS score; SD-OCT; fluorescein angiography; those evaluating the secondary objective of pharmacokinetics including plasma exposure of UBX1325 and UBX0601; and those evaluating the exploratory endpoints of pharmacodynamic effects including BCVA, SD-OCT and DRSS scores.

The primary objective of the study was to assess the local and systemic safety, tolerability, maximum tolerated dose and incidence of DLTs of UBX1325 following a single intravitreal treatment in patients with DME and/or patients with nAMD. Safety was evaluated throughout the study assessed by full clinical evaluation of the anterior and posterior segment by direct ophthalmologic evaluation, indirect ophthalmoscopy, determination of any changes in intraocular pressure after injection, assessment of any abnormalities in color fundus photography (including DRSS score), structural changes in retinal architecture/thickness by SD-OCT, vessel abnormalities, leaking or bleeding by fluorescein angiography. Each of these were evaluated by the principal investigator and an independent specialty reading center. A SAC included an independent ophthalmology retinal expert and members of the study team to assess all TEAEs and all safety data during the study as well as discuss each patient with the respective principal investigator. The SAC was required to approve all dose-escalation determinations.

The secondary objective of the study was to characterize systemic pharmacokinetics of UBX1325 and its active parent molecule, UBX0601. Exploratory objectives were set to explore potential pharmacodynamic effects of UBX1325 through multiple endpoints such as BCVA, SD-OCT and DRSS scores by color fundus photography. The study was performed in accordance with the current version of the Declaration of Helsinki (52nd WMA General Assembly, Edinburgh, Scotland, October 2000). The trial was conducted in agreement with the International Conference on Harmonisation guidelines on Good Clinical Practice.

Trial statistical analysis

The sample size was not based on statistical considerations. Each UBX1325 dose cohort enrolled three patients. The total number of participants enrolled in the study was based on the number of dose cohorts reached and the occurrence of DLTs for each dose cohort and the number of dose escalations required to achieve the maximum tolerated dose. All study parameters were listed with parameters of special interest summarized descriptively by dose cohort and overall and included number of participants, mean, standard deviation, median, minimum and maximum for continuous parameters, and frequency and percentage for categorical parameters. All results are expressed as the mean ± s.e.m. unless indicated otherwise. The clinical trial statistical analysis plan is provided in Supplementary Note 3.

Statistical analysis of non-trial data

All experiments were performed at least three independent times and obtained similar results. Biological replicates (n) for each experiment are indicated in the figure legends and refer to each experimental group. All results were analyzed in a masked manner and are expressed as the mean ± s.e.m. unless indicated otherwise and are considered statistically significant when $P < 0.05$. Two conditions were analyzed using Student's t-test (two-tailed). More than two conditions or groups were analyzed using one-way ANOVA at a single time point and using two-way ANOVA when over a time course. Statistical analyses were obtained with the Prism (v9) software.

Reporting summary

Further information on research design is available in the Nature Portfolio Reporting Summary linked to this article.

Data availability

Requests for additional information, reagents or material resources should be addressed to P.S. Sequencing data from STZ-treated mouse retinas have been deposited in NCBI's Gene Expression Omnibus under accession number GSE211583. Datasets used to perform single-cell transcriptomic analyses on mouse diabetic retinas were previously published and are publicly available under the accession number GSE178121. Datasets used to perform bulk transcriptomic analyses on rat diabetic retinas were previously published and are publicly available under the accession number GSE20886. All information on materials and reagents is provided in Supplementary Information. All clinical data have been provided in the paper in the form of figures, in the text or in Supplementary Information (including the clinical trial protocol,

STROBE checklist and the statistical analysis plan). Additional requests for clinical data should be addressed to the corresponding author and may be provided upon reasonable request. Source data are provided with this paper.

References

65. Mattapallil, M. J. et al. The Rd8 mutation of the *Crb1* gene is present in vendor lines of C57BL/6N mice and embryonic stem cells, and confounds ocular induced mutant phenotypes. *Invest. Ophthalmol. Vis. Sci.* **53**, 2921–2927 (2012).
66. Melsted, P. et al. Modular, efficient and constant-memory single-cell RNA-seq preprocessing. *Nat. Biotechnol.* **39**, 813–818 (2021).
67. Hao, Y. et al. Integrated analysis of multimodal single-cell data. *Cell* **184**, 3573–3587 (2021).
68. Skinnider, M. A. et al. Cell type prioritization in single-cell data. *Nat. Biotechnol.* **39**, 30–34 (2021).
69. Hanzelmann, S., Castelo, R. & Guinney, J. GSVA: gene set variation analysis for microarray and RNA-seq data. *BMC Bioinformatics* **14**, 7 (2013).
70. Liberzon, A. et al. The Molecular Signatures Database (MSigDB) hallmark gene set collection. *Cell Syst.* **1**, 417–425 (2015).

Acknowledgements

P.S. holds the Wolfe Professorship in Translational Research, a Canada Research Chair in Retinal Cell Biology as well as the Fonds de Recherche en Ophtalmologie de l'Université de Montréal Endowed Chair. S.C.-G. holds a fellowship from the Fonds de Recherche du Québec - Santé (FRQ-S) and the Montreal Diabetes Research Center. This work was supported by UNITY Biotechnology. Other funding was provided from operating grants to P.S. from Diabetes Canada (DI-3-18-5444-PS), the Canadian Institutes of Health Research (Foundation grant 353770), The Alcon Research Institute Senior Investigator Award and The Heart and Stroke Foundation of Canada (G-16-00014658) and BrightFocus Foundation (M2022015I). Additional support was provided by the Fonds de Recherche en Ophtalmologie de l'Université de Montréal (FROUM), the Réseau en Recherche en Santé de la Vision (RRSV) and the FRQ-S/RRSV-funded Single-Cell Academy. We thank V. Guber for the management of the mouse colony, the research assistants at the animal facilities, and M. Sergeev at the microscope core facilities of the Hospital Maisonneuve-Rosemont Research Center for all their technical support throughout the duration of this project. We also thank H. Findlay and G. Mawambo for the technical assistance provided, and B. Larrivée for reagents.

Author contributions

P.S., S.C.-G., J. Dananberg, A.G. and L.S. designed the study with contribution from P.R.T.; S.C.-G., F.F., R.D.-M., G.C., G.B., I.H., R.R., R.J. and P.P. performed research; F.A.R. provided human specimens; S.C.-G., F.F., R.D.-M., G.C., G.B., R.R., M.B., A.D., S.C., P.P., P.R.T., P.J.B. and P.S. analyzed data; S.C.-G. prepared the figures; P.S. and S.C.-G. wrote the paper with contributions from P.R.T., A.G., F.A.M., S.K., D.R., J. Dananberg, P.J.B., A.M.W. and M.H. All authors revised and approved the submitted version of the paper.

Competing interests

P.S., J. Dananberg, A.G., L.S. and A.N. are executives at UNITY Biotechnology. N.D. is the founder of UNITY Biotechnology. S.K., D.R., L.M., P.P., P.J.B., A.N., J.D., L.S. and P.R.T. were employees of UNITY Biotechnology during the time this project was developed and hold shares in the company. S.C.-G., R.D.-M., F.F., G.C., A.D., A.M.W. and J.-S.J. have contract work with UNITY Biotechnology. The other authors declare no competing interests.

Additional information

Extended data is available for this paper at https://doi.org/10.1038/s41591-024-02802-4.

Supplementary information The online version contains supplementary material available at https://doi.org/10.1038/s41591-024-02802-4.

Correspondence and requests for materials should be addressed to Przemyslaw Sapieha.

Peer review information *Nature Medicine* thanks William Keyes and the other, anonymous, reviewer(s) for their contribution to the peer review of this work. Primary Handling Editor: Michael Basson, in collaboration with the *Nature Medicine* team.

https://doi.org/10.1038/s41591-024-02802-4

Extended Data Table 1 | DME and nAMD patients enrolled in NCT04537884 and treated with UBX1325 (demographics).

	Dose	Age	Sex	Ethnicity	Race
DME	0.5µg	78	F	Not Hispanic or Latino	White
	0.5µg	64	F	Not Hispanic or Latino	White
	1.0µg	76	M	Not Hispanic or Latino	White
	1.0µg	69	F	Hispanic or Latino	White
	5.0µg	74	M	Hispanic or Latino	White
	5.0µg	62	M	Hispanic or Latino	Black or African American
	10.0µg	56	M	Not Hispanic or Latino	White
	10.0µg	68	M	Hispanic or Latino	White
nAMD	0.5µg	78	M	Not Hispanic or Latino	White
	1.0µg	73	F	Not Hispanic or Latino	White
	5.0µg	76	M	Not Hispanic or Latino	Asian
	10.0µg	85	F	Not Hispanic or Latino	White
	10.0µg	63	F	Not Hispanic or Latino	White
	10.0µg	90	M	Not Hispanic or Latino	White
	10.0µg	76	M	Hispanic or Latino	White
	10.0µg	82	F	Not Hispanic or Latino	White
	10.0µg	78	M	Not Hispanic or Latino	White
	10.0µg	69	F	Not Hispanic or Latino	White
	10.0µg	75	F	Not Hispanic or Latino	White

DME = Diabetic macular edema; F = Female; M = Male; nAMD = neovascular age-related macular degeneration

DME and nAMD patients enrolled in NCT04537884 and treated with UBX1325 (demographics).

nature portfolio

Corresponding author(s): Przemyslaw SAPIEHA

Last updated by author(s): January 1st, 2024

Reporting Summary

Nature Portfolio wishes to improve the reproducibility of the work that we publish. This form provides structure for consistency and transparency in reporting. For further information on Nature Portfolio policies, see our Editorial Policies and the Editorial Policy Checklist.

Statistics

For all statistical analyses, confirm that the following items are present in the figure legend, table legend, main text, or Methods section.

n/a	Confirmed
☐	☒ The exact sample size (*n*) for each experimental group/condition, given as a discrete number and unit of measurement
☐	☒ A statement on whether measurements were taken from distinct samples or whether the same sample was measured repeatedly
☐	☒ The statistical test(s) used AND whether they are one- or two-sided *Only common tests should be described solely by name; describe more complex techniques in the Methods section.*
☒	☐ A description of all covariates tested
☐	☒ A description of any assumptions or corrections, such as tests of normality and adjustment for multiple comparisons
☐	☒ A full description of the statistical parameters including central tendency (e.g. means) or other basic estimates (e.g. regression coefficient) AND variation (e.g. standard deviation) or associated estimates of uncertainty (e.g. confidence intervals)
☐	☒ For null hypothesis testing, the test statistic (e.g. *F*, *t*, *r*) with confidence intervals, effect sizes, degrees of freedom and *P* value noted *Give P values as exact values whenever suitable.*
☒	☐ For Bayesian analysis, information on the choice of priors and Markov chain Monte Carlo settings
☒	☐ For hierarchical and complex designs, identification of the appropriate level for tests and full reporting of outcomes
☒	☐ Estimates of effect sizes (e.g. Cohen's *d*, Pearson's *r*), indicating how they were calculated

Our web collection on statistics for biologists contains articles on many of the points above.

Software and code

Policy information about availability of computer code

Data collection	Microscopy data was obtained using the Zen Blue edition 3.2 software on a Zeiss Axio Imager Z2 microscope. Transcellular electrical resistance was collected using the ECIS (v1.2) software from Applied Biophysics. ERG data in mouse was collected using a UTAS-E Visual Electrodiagnostic Test System. Clinical data was collected with an electronic data capture (EDC) system customized by the Sponsor.
Data analysis	Protein expression in human eye globes were quantified using the Visiopharm image analysis software. Whole-tissue RNA-sequencing data was analyzed with Torrent Suite software v5.4.0. Single-cell RNA-sequencing data was analyzed using the kb-python v0.27.4 (read alignment), Seurat (v5), Augur (v1) and Gene Set Variation Analysis (GSVA v1.51.1) softwares. Quantification of protein signal in immunohistochemistry and Western blot were obtained with ImageJ (v2.3.0). Statistical analyses were obtained with the Prism (v9) software.

For manuscripts utilizing custom algorithms or software that are central to the research but not yet described in published literature, software must be made available to editors and reviewers. We strongly encourage code deposition in a community repository (e.g. GitHub). See the Nature Portfolio guidelines for submitting code & software for further information.

Data

Policy information about availability of data

All manuscripts must include a data availability statement. This statement should provide the following information, where applicable:

- Accession codes, unique identifiers, or web links for publicly available datasets
- A description of any restrictions on data availability
- For clinical datasets or third party data, please ensure that the statement adheres to our policy

Requests for additional information, reagents or material resources should be addressed to Przemyslaw Sapieha (PS) by email at mike.sapieha@umontreal.ca. Sequencing data from STZ-treated mouse retinas has been deposited in NCBI's Gene Expression Omnibus (GEO) under the accession number GSE211583. Data sets used to perform single cell transcriptomic analyses on mouse diabetic retinas were previously published and are publicly available under the accession number GSE178121. Data sets used to perform bulk transcriptomic analyses on rat diabetic retinas were previously published and are publicly available under the accession number GSE20886. All information on materials and reagents is provided the online supplementary resources online (supplementary information). All clinical data has been provided in the manuscript in form of figures, in the text or in the supplementary resources online (including the clinical trial protocol, STROBE checklist and the statistical analysis plan). Additional requests for clinical data should be addressed to the corresponding author (mike.sapieha@umontreal.ca) and may be provided upon reasonable request.

Research involving human participants, their data, or biological material

Policy information about studies with human participants or human data. See also policy information about sex, gender (identity/presentation), and sexual orientation and race, ethnicity and racism.

Reporting on sex and gender	Sex of the participants was considered and is reported in corresponding tables and supplementary/extended tables. Gender was not considered in this study.
Reporting on race, ethnicity, or other socially relevant groupings	Race and ethnicity are reported in the document Extended Data Table 1 (demographics). These were not considered during the analyses. No additional socio-cultural information was considered in the study.
Population characteristics	The major inclusion criteria were: Age ≥18 years; evidence of non-proliferative diabetic retinopathy who were, in the opinion of the investigator, inadequately responding to, unlikely to benefit from, or had failed current treatment options; presence of center-involved DME with central subfield thickness (CST) ≥ 350µm on SD-OCT at Day 1; BCVA at Screening and on Day 1 in the study eye of 55 ETDRS letters (approximately equivalent to 20/80 on the Snellen chart) or worse. Major exclusion criteria were: Concurrent disease in the study eye or structural damage, other than DME or nAMD, that could compromise or BCVA improvement; HbA1C ≥ 12 and/or recent signs of uncontrolled diabetes; history of vitreous hemorrhage in the study eye within 2 months prior to Screening; concomitant therapy with anti-VEGF therapies or previous use of these agents in the study eye within 90 days of enrolment; use of systemic and intraocular steroid use for 6 months prior to enrolment. Age, ethnicity and race are described in the tables and supplementary tables.
Recruitment	After a patient was identified as potentially eligible for the study, the patient was invited to participate. If the patient agreed to study participation, written informed consent was obtained before any study-specific procedures are performed. Patients who consented to participate in the study were assigned a screening number. After each eligible subject consented, the site staff obtained a UBX1325 dose assignment and a unique subject number. Following receipt of the subject number and dose assignment, the site staff prepared the Study Drug as instructed by the Pharmacy Manual.
Ethics oversight	The study was performed in accordance with the current version of the declaration of Helsinki (52nd WMA General Assembly, Edinburgh, Scotland, October 2000). The trial was conducted in agreement with the International Conference on Harmonisation (ICH) guidelines on Good Clinical Practice (GCP). The study gained regulatory approval from the US Food and Drug Administration (FDA) on August 25, 2020, conducted under a US Investigational New Drug (IND) number 145348. The study gained full approval from the central Institutional Review Board (IRB), Advarra, on August 6, 2020. Oversight for the study was done through a Safety Assessment Committee (SAC) that met to review all safety data following any sentinel dosing and after completion of a dosing cohort. At each meeting, the Principal Investigators or their designee were available to answer questions and describe any observed findings. Each dose escalation required formal SAC approval.

Note that full information on the approval of the study protocol must also be provided in the manuscript.

Field-specific reporting

Please select the one below that is the best fit for your research. If you are not sure, read the appropriate sections before making your selection.

☒ Life sciences ☐ Behavioural & social sciences ☐ Ecological, evolutionary & environmental sciences

For a reference copy of the document with all sections, see nature.com/documents/nr-reporting-summary-flat.pdf

Life sciences study design

All studies must disclose on these points even when the disclosure is negative.

Sample size	Power analyses were previously established in our laboratories for all models used in this study. Our laboratories have worked extensively with the models and paradigms presented in this study.
Data exclusions	Diabetic mice (STZ-injected) that lost more than 20% of their initial body weight or did not reach at least 17-25mM blood glucose were excluded from the study. Mice where intravitreal injection pierced the lens or led to bleeding were excluded. Western blot samples where transfer was defective or partial were excluded.
Replication	All experiments were performed at least 3 independent times.
Randomization	Animals and/or cells were randomized in a blinded manner into different treatment groups at the beginning of each experiment.
Blinding	Investigators that analyzed the data were blinded to the identity of the group when experimental design allowed. Several experiments on vascular permeability and electrophysiology were repeated and conducted in distinct laboratories (University of Montreal and CRO Vanderbilt Ocular) to ensure reproducibility.

Reporting for specific materials, systems and methods

We require information from authors about some types of materials, experimental systems and methods used in many studies. Here, indicate whether each material, system or method listed is relevant to your study. If you are not sure if a list item applies to your research, read the appropriate section before selecting a response.

Materials & experimental systems

n/a	Involved in the study
☐	☒ Antibodies
☐	☒ Eukaryotic cell lines
☒	☐ Palaeontology and archaeology
☐	☒ Animals and other organisms
☐	☒ Clinical data
☒	☐ Dual use research of concern
☒	☐ Plants

Methods

n/a	Involved in the study
☒	☐ ChIP-seq
☒	☐ Flow cytometry
☒	☐ MRI-based neuroimaging

Antibodies

Antibodies used

All antibodies (primary and secondary) and references are compiled in the Supplementary Table S6 of the manuscript's supplementary resources only. All dilutions used are indicated in the table depending on the type of experiment (IHC, ICC, WB, etc.).

PRIMARY ANTIBODIES
Antibody against; Species; Application; Company; Catalog #
ALB; Goat; IHC (1:100); Bethyl Labs; A90-234A
β-actin; Mouse; WB (1:10000); Cell Signaling; 3700
β-catenin; Mouse; ICC (1:50); BD Biosciences; 610153
BCL-2 (Clone D17C4) custom carrier-free; Rabbit; Target Eng.; Cell Signaling; 3498BF
BCL-2; Rabbit; IHC (1:100); Abcam; ab182858
BCL-xL (Clone 54H6) custom carrier-free; Rabbit; Target Eng.; Cell Signaling; 2764BF
BCL-XL; Rabbit; IHC (1:100); Cell Signaling; 2764
BIM (Clone C34C5), custom carrier-free Rabbit Target Eng.; Cell Signaling; 2933BF
COL4; Rabbit; IHC (1:100); Abcam; ab6586
ISOLECTIN-B4 (IB4) Fluorescein-conjug.; G. simplicifolia; IHC (1:100); Vector FL-1101
gammaH2Ax; Mouse; WB (1:2500); Sigma-Aldrich; 05-636
PAI1; Mouse; WB (1:5000) and IHC (1:100); Santa Cruz; sc-5297
PML; Mouse; ICC (1:200); Santa Cruz; sc-966
p16INK4A; Mouse; IHC; (manuf.); Roche; 705-4793
p16INK4A; Rabbit; WB (1:2000) Abcam; ab211542
p21; Rabbit; WB; (1:2000); Abcam; ab109199
p53; Rabbit; WB (1:5000); Abcam; ab131442
OCLN; Rabbit; WB (1:5000); ThermoFisher; 33-1500
VE-Cadherin; Goat; ICC (1:75); Santa Cruz; sc-6458
VE-Cadherin; Mouse; WB (1:1000); Santa Cruz; sc-9989
p-VE-Cadherin; Rabbit; WB (1:1000); Abcam; ab119785

SECONDARY ANTIBODIES
AF488 anti-Mouse; Donkey; IHC (1:2000) and ICC (1:5000); Invitrogen; A21202
AF488 anti-Mouse Goat IHC (1:2000) Invitrogen A11001

AF488 anti-Rabbit; Donkey IHC (1:2000) Invitrogen A21206
AF594 anti-Goat; Donkey; IHC (1:2000) and ICC (1:5000); Invitrogen A11058
AF647 anti-Mouse; Goat IHC (1:2000); Invitrogen; A21235
AF647 anti-Rabbit; Donkey; IHC (1:2000); Invitrogen; A31573
HRP anti-Mouse; Donkey; WB (1:10000); Amersham; LNA931V
HRP anti-Rabbit; Donkey; WB (1:10000); Amersham; LNA934V

Validation

When possible, we used KO-validated antibodies and that were compatible (tested by manufacturer) with the technique employed. We used isotype control for internal validation of the antibodies when required.

Eukaryotic cell lines

Policy information about cell lines and Sex and Gender in Research

Cell line source(s)	Human retina microvascular endothelial cells (HRMECs) were purchased at CellSystems (#ACBRI181) or Neuromics (#HEC09). MCF-7 cells were purchased at ATCC (#HTB-22).
Authentication	All cell lines were authentified and certified by the vendor and verified by morphology at a regular basis in the laboratory.
Mycoplasma contamination	Annually, all cell lines in culture were tested for mycoplasma contamination and all results have been reported as negative.
Commonly misidentified lines (See ICLAC register)	No commonly misidentified lines were used in this study.

Animals and other research organisms

Policy information about studies involving animals; ARRIVE guidelines recommended for reporting animal research, and Sex and Gender in Research

Laboratory animals	STZ-induced diabetes and oxygen-induced retinopathy was elicited in C57Bl/6J mice at 6 weeks (STZ) old or 7 days old (OIR), respectively. Pups in hyperoxia chamber were nursed by CD1 mothers (>4 weeks old). All mice were housed in 12h-12h light-dark cycles, 23-25ºC and a relative humidity (around 50%) in ventilated cages.
Wild animals	The study did not involve wild animals.
Reporting on sex	Sex is reported in the methods. Diabetes was induced with STZ injections only in males mice since females have resistance to the chemical and do not develop diabetes.
Field-collected samples	The study did not involve samples collected in the field.
Ethics oversight	All animal experimentation was previously approved by local ethical authorities at either the Hospital Maisonneuve-Rosemont (CPA protocol 2019-1877), at UNITY Biotechnology or at the Vanderbilt Ocular (VO)-CRO hired by UNITY Biotechnology. Animal experiments were also adhered to the ARRIVE guidelines and to the ARVO statement for the use of animals in ophthalmic and vision research.

Note that full information on the approval of the study protocol must also be provided in the manuscript.

Clinical data

Policy information about clinical studies

All manuscripts should comply with the ICMJE guidelines for publication of clinical research and a completed CONSORT checklist must be included with all submissions.

Clinical trial registration	NCT04537884
Study protocol	https://clinicaltrials.gov/ct2/show/NCT04537884
Data collection	An electronic data capture (EDC) system was designed and managed on behalf of the Sponsor by the Sponsor's designated contract research organization. Clinical data was entered by study site personnel within 5 business days of the subject visit or activity conduct. Monitoring of the study was conducted on site by a designee of the Sponsor who conducted document and source data review, as well as remote data monitoring in the intervals between monitoring visits. Data was reviewed remotely by the Medical Monitor for safety oversight. All study-related information was recorded on source documents. All required study data were recorded in the electronic Case Report Forms (eCRFs). All eCRF data was required to be submitted to the Sponsor throughout and at the end of study in a timely and accurate manner. The data was checked for completeness and correctness in real-time online by the Sponsor.
Outcomes	Primary outcomes were safety and tolerability. Secondary outcomes were plasma concentration of UBX1325 following a single intravitreal injection [Time Frame: up to 24 hours post dose]. Exploratory outcome measures were: BCVA, anterior and posterior segment evaluation and ophthalmoscopy, intra-ocular pressure, color fundus photography, Diabetic Retinopathy Severity Scale (DRSS) score; Spectral Domain-Optical Coherence Tomography (SD-OCT); fluorescein angiography (FA).

Plants

Seed stocks	No seed stocks were used or generated.
Novel plant genotypes	No novel plant genotypes were generated.
Authentication	Authentication procedures were not required.